Vav2 regulates dopamine transporter-dependent mesolimbic dopamine homeostasis and behavioral responses to cocaine

Shuyong Zhu,[1,7,#] Chengjiang Zhao,[1,2,7] Yingying Wu,[1,2,7] Qiaoqiao Yang,[1,3] Aiyun Shao,[1] Tiepeng Wang,[1] Jianfu Wu,[1] Yanqing Yin,[1] Yandong Li,[1] Jincan Hou, [1] Xinhua Zhang, [1,4] Guomin Zhou,[3] Xiaosong Gu,[4] Xiaomin Wang,[5] Xosé R. Bustelo,[6] Jiawei Zhou,[1*]

[1] Institute of Neuroscience, State Key Laboratory of Neuroscience, CAS Center for Excellence in Brain Science, Shanghai Institutes for Biological Sciences, Chinese Academy of Sciences, Shanghai, 200031, China

[2] University of Chinese Academy of Sciences, Shanghai 200031, China.

[3] Department of Anatomy, Histology and Embryology, Shanghai Medical School, Fudan University, Shanghai, 200032, China

[4] Center for Joint Creation, Department of Anatomy, School of Medicine, Nantong University, JS, 226001, China

[5] Center of Parkinson's Disease, Beijing Institute for Brain Disorders, Beijing, 100053, China

[6] Centro de Investigación del Cáncer/Cancer Research Center, CSIC-University of Salamanca, Campus Unamuno, E-37007 Salamanca, Spain

[7] These authors contributed equally to this work

Running Head: Vav2 regulates mesolimbic DAT trafficking and activity

[*]Corresponding Author:

Jiawei Zhou, Ph.D.
Institute of Neuroscience
Chinese Academy of Sciences
320 Yueyang Road
Shanghai, 200031
China

Phone/ Fax: +86-21-5492 1073

Email: jwzhou@ion.ac.cn

URL: www.ion.ac.cn/laboratories/int.asp?id=53

Present address: Institute of Virology, Hannover Medical School, Hannover, Germany

Key words:

Vav2; dopaminergic neuron; dopamine transporter; cocaine; reward; mesolimbic pathway, GDNF; Ret; trafficking

Abstract

Dopamine (DA) homeostasis is essential for a variety of brain activities. Dopamine transporter (DAT)-mediated DA reuptake is one of the most critical mechanisms for the control of normal DA homeostasis. However, the molecular mechanisms underlying the regulation of DAT activity in the brain remain poorly understood. Here, we showed that a Rho family GEF protein Vav2 controls DAT cell surface expression and transporter activity through internalization of a protein complex, consisting of Vav2, glial cell line-derived neurotrophic factor cognate receptor Ret and DAT. Mice deficient in either *Vav2* or *Ret* displayed an elevation of DAT activity, resulting in a significant increase in the intracellular DA levels selectively in the nucleus accumbens. *Vav2*$^{-/-}$ mice exposed to cocaine showed reduced DAT activity and diminished behavioral cocaine response. Our data identify Vav2 as a critical regulator of DAT trafficking *in vivo* and a determinant of DA homeostasis in limbic DA neuron terminals.

Introduction

Dopamine (DA) has long been known to play a major role in diverse brain functions including movement coordination, reward, learning and memory. Dysfunction in dopaminergic (DA) systems is associated with a variety of neurological disorders, such as psychiatric diseases, attention-deficit/hyperactivity disorder and Parkinson's disease. The significant impact of dysfunction of DA system on health indicates the importance of maintaining DA functionality through homeostatic mechanisms that are largely dependent on the delicate balance between synthesis, storage, release, reuptake and metabolism. DA signaling is highly regulated in a temporal and spatial fashion. After released into the synaptic cleft, DA is quickly removed by dopamine transporter (DAT) which is central to terminate DA signaling and maintain DA homeostasis in single dopaminergic neuron terminals. As such, $DAT^{-/-}$ mice display dramatic DA depletion in tissue stores and hyperlocomotion[1]. DAT is also known as the primary target for the addictive drugs cocaine and amphetamine. Thus, an understanding of the molecular mechanisms underlying control of DAT expression and activity is likely to have a significant impact on DA signaling and DAT-associated brain disorders.

The function of DAT can be regulated through redistribution of the protein to or from the cell surface. Much has been learned in recent years about the mechanisms underlying DAT trafficking which has been characterized mostly thoroughly by studying the DAT-interacting proteins in culture. Thus, a set of proteins, such as protein kinase C[2 3, 4], PICK1[5], Hic-5[6], calcium/calmodulin-dependent kinase II[7], flotilin-1[8] and Rin GTPase[9], that mediate DAT trafficking has been identified. Although these studies have provided much insight into the

protein machinery involved in DAT trafficking, the majority of these studies has been performed predominantly in heterologous systems. As a consequence, the functional significance of many observations has not been evaluated in brain *in vivo* and the specific mechanisms of DAT internalization remain to be fully defined.

Recently Vav2 was described as potential mediator of endocytosis[10, 11]. Vav2 belongs to the VAV family of oncogene proteins with guanine nucleotide exchange factor (GEF) activity for small G proteins of the Rho family. Vav family comprises three distinct genes (*Vav1-3*). Unlike Vav1 which is exclusively expressed in hematopoietic cells, Vav2 and Vav3 are broadly expressed in embryonic and postnatal tissue[12, 13]. These two proteins are essential for proper signaling responses in cytoskeletal organization, mitogenesis, neuronal morphogenesis during development and other biological processes[10, 13-15]. Vav proteins contain multiple subdomains including Src-homology domains 2 and 3 (SH2 and SH3, respectively) and a guanine nucleotide releasing factor-like domain, each of which exhibits distinctive features. The SH2 and SH3 domains function as molecular adhesives linking cell surface receptor and downstream signaling proteins. The guanine nucleotide releasing factor-like domain can be quickly triggered by direct interaction with several ligand-activated transmembrane tyrosine kinase, such as epidermal growth factor (EGF) receptor and ephrin[10, 16]. Tyrosine phosphorylation of Vav triggers the activation of Vav GDP/GTP exchange activity that stimulates Rho and Rac GTPases[17]. Previous studies have shown that deficiency of *Vav3* causes a significant increase in the concentration of plasma DA, whereas loss of *Vav2* results in elevated plasma concentrations of noradrenaline (NE) and adrenaline[18, 19]. Given that

Vav2/3 are expressed in developing and adult brain[10, 11, 15] and loss of Vav2/3 perturbs the balance of catecholamine in the peripheral sympathetic nervous system[18, 19], we hypothesize that Vav proteins may also play a role in the control of steady-state levels of catecholamine in the brain.

In this study, Vav2 was identified as a crucial component promoting limbic DAT internalization via glial cell line-derived neurotrophic factor (GDNF) signaling. We demonstrated that loss of Vav2 led to an abnormal accumulation of DAT in plasma membrane, resulting in disrupted DA homeostasis in DA neuron terminals, and impaired response to cocaine-induced behaviors. Our data indicate an essential role of Vav2 in regulating the functionality of mesolimbic DA system.

Results

Vav2 protein is preferentially expressed in adult VTA in the midbrain

Immunoblot analysis revealed a heterogeneous expression of Vav2 in adult mouse brain with the highest levels in the ventral tegmental area (VTA) and olfactory bulb (OB) among the major brain regions examined, such as the nucleus accumbens (NAc), dorsal striatum (dSTR) and cerebrocortex (**Fig. 1a, b**). To dissect these brain regions more precisely, transgenic mice expressing green fluorescent protein (GFP) under the control of tyrosine hydroxylase (TH)-promoter[20] were employed. We found that Vav2 expression was remarkably higher in the VTA than in the substantia nigra (SN) at various stages in brain development [postnatal day 14 (P14) and adult] (**Fig. 1c**, **d** and **Supplementary Fig. 1a**, **b**), whereas in the SN, Vav2 expression levels declined with advancing of age, consistent with developmental expression profile of Vav2 in whole brain lysates shown by others[10]. Further Western blotting analysis on the synaptosomes prepared from the NAc and dSTR showed that the levels of synaptosomal Vav2 protein in the NAc were 2.46-fold higher than in the dSTR (**Fig. 1e, f)**. Vav2 *in situ* hybridization combined with immunohistochemistry for TH performed in adult mouse brain sections showed that Vav2 hybridization signals were localized in TH+ neurons in both the VTA and SN (**Fig. 1g**). Some TH+ neurons in both the VTA and SNc co-expressed Vav2 protein as revealed by double-labeled immunofluorescent staining (**Fig. 1h**). These results suggest that Vav2 displays distinct expression pattern from Vav3 in brain (**Supplementary Fig. 1c**) with preferential expression in VTA DA neurons.

Pronounced elevation in levels of DA and 5-HT, but not of NE, in the NAc of *Vav2*$^{-/-}$ mice

To unravel the potential function of Vav2 in the DA neuron systems, we measured the catecholamine concentrations in the NAc and dSTR of adult mice using high-performance liquid chromatography (HPLC). As shown in **Fig. 1i-k**, the levels of DA and 5-hydroxytryptamine (5-HT), but not of NE, in the NAc of *Vav2*$^{-/-}$ mice were markedly elevated (~150%) compared with their wild-type (WT) counterparts, albeit that the levels of DA metabolites 3,4-dihydroxyphenylacetic acid (DOPAC), homovanillic acid (HVA) and 5-HT metabolite 5-hydroxyindoleacetic acid (5-HIAA) remained unchanged. **This may be an indication that the mutation has no influence on DA release that would likely result in a parallel increase in DOPAC.** However, the alteration of DA levels was not seen in the dSTR or OB of *Vav2*$^{-/-}$ mice (**Fig. 1l-n** and **Supplementary Fig. 1d**). Likewise, ablation of *Vav3* did not result in a significant alteration in the concentrations of catecholamines in both the NAc and dSTR (**Supplementary Fig. 1e, f**). No significant morphological alteration in the mesolimbic and mesostriatal pathways of either *Vav2*$^{-/-}$ mice was observed (**Supplementary Fig. 1g, h**). Taken together, these results suggest that Vav2 is required for the maintenance of DA homeostasis in limbic DA neuron terminals in a brain region-specific manner.

DAT plays a role in both extracellular clearance of DA and steady state tissue levels of DA[21]. We thus first evaluated the impact of *Vav2* ablation on the DA uptake. [^{3}H]DA radioassay revealed that genetic deletion of *Vav2* resulted in ~60% increase of DAT-mediated DA uptake on synaptosomal preparations from the NAc, but not from the dSTR. This effect could be rescued by adeno-associated virus (AAV)-mediated overexpression of Vav2 selectively in the VTA, but not SN (**Fig. 2a, b** and **Supplementary Fig. 1i)**. In contrast, *Vav3*

ablation had no impact on DAT activity (**Supplementary Fig. 1j**)**.** Similarly, either knock-down of Vav2 or overexprssion of Vav2 L212Q mutant, the dominant negative form of Vav2 GEF activity[22], caused an increase in [^{3}H]DA reuptake in HEK293 cell line stably expressing yellow fluorescent protein (YFP)-tagged DAT (**Fig. 2c, Supplementary Fig. 1k**). Moreover, knock-down of Vav2 caused the same effect in the Neuro 2A (N2a) mouse neural crest-derived cell line stably expressing both red fluorescent protein (RFP)-tagged DAT and GDNF co-receptor GFRα1 (**Fig. 2d, e**), as shown in the HEK293 cells, and this effect could be rescued by co-expression of RFP-tagged human Vav2 (**Fig. 2e**). These results collectively support the idea that Vav2 functions as a negative regulator of DAT activity in a GEF activity-dependent manner. Further biochemical analysis showed normal degradation of DA with reduced DA biosynthesis in the absence of *Vav2* (**Supplementary Fig. 2a-l**), which may result from aberrantly high DA levels as a negative feedback inhibition.

Vav2 negatively regulates DAT surface expression

The upregulation of DAT transporter activity in *Vav2*$^{-/-}$ mice suggests enhanced surface expression of DAT. To test this, synaptosomes from both genotypes were biotinylated and immunoblotted using the specific anti-DAT antibody. As shown in **Fig. 2f, g**, the levels of biotinylated DAT were markedly increased (~70%) in the NAc of *Vav2*$^{-/-}$ mice relative to WT mice, while in the dSTR, the surface DAT expression showed no significant changes between genotypes. In either case, the total DAT levels remained unchanged between genotypes (**Supplemental Fig. 8a**). Likewise, in HEK293 cells, either knock-down or overexpression of Vav2 or its constitutive active form (Vav2 Y172F mutant) also markedly altered DAT surface

expression levels (**Fig. 2h, i**), but not the total DAT levels (**Supplemental Fig. 8b, c**). Consistent with these results, DAT maximal velocity (V_{max}) of [^{3}H]DA uptake was significantly higher in the NAc of *Vav2* KO mice than that in WT control (WT, 30.845 ±0.806 pmol/mg protein/min; KO, 51.290 ±4.045 pmol/mg protein/min, $P < 0.05$) with no significant changes in the K_m value (34.45 ± 2.485 versus 43.96 ± 9.067 nmol, $P > 0.05$, **Fig. 2j**). These results suggest that the synaptosomal DAT transporter activity is largely regulated by Vav2-mediated membrane trafficking. Moreover, the synaptosomal DAT activity is regulated by phosphorylation of DAT[23, 24] in addition to membrane trafficking[25-27]. To clarify the contribution of DAT phosphorylation to Vav2-mediated DAT regulation, we analyzed the DAT phosphorylation by using the threonine[53]-phosphospecific antibody, since the DAT phosphorylation site threonine[53] regulates substrate reuptake and amphetamine-stimulated efflux [28, 29]. As shown in **Supplementary Fig. 2m, n**, the threonine[53] phosphorylation levels of DAT in the NAc, dSTR and VTA showed no significant changes between genotypes, supporting the idea that DAT phosphorylation is not involved in Vav2-mediated DAT trafficking. **Notably, DAT was not co-immunoprecipitated with Vav2 in VTA tissue lysates from adult mouse brain, although co-IP assays showed interaction between exogenous DAT and Vav2 in cell lines (data not shown).**

Vav2 is a substrate of Ret receptor tyrosine kinase.

Next, we sought to determine the mechanisms by which Vav2 is activated in the regulation of DAT function. Recent studies showed selective enhancement of DAT activity in the NAc of *GDNF*$^{+/-}$ mice[30], which resembles the phenotypes observed in *Vav2*$^{-/-}$ mice (**Fig.**

2). This led us to hypothesize that Vav2 may be functionally related to GDNF signaling. To test the hypothesis, we first assessed the DA tissue levels and DAT activity in *Ret*$^{+/-}$ mice, since Ret is a cognate receptor for GDNF with transmembrane tyrosine receptor kinase (RTK) activity[31]. In accordance with the biochemical changes observed in *Vav2*$^{-/-}$ mice, there were significant increases in DA uptake in the synaptosomes from the ventral, but not dorsal, striatum of *Ret*$^{+/-}$ mice (**Fig. 3a**). This was accompanied with a significant increase in the levels of DAT surface expression (**Fig. 3b, c**), while the total DAT levels were not significantly altered (**Supplmentary Fig. 8d**). We also found selective augmentation of tissue DA levels in the NAc, but not dSTR and OB, of *Ret*$^{+/-}$ mice (**Fig. 3d, e** and **Supplementary Fig. 3a**). Consistent with **Supplementary Fig. 2m, n**, *Ret*$^{+/-}$ mice showed no marked alteration in the levels of Thr^{53} DAT expression (**Supplementary Fig. 3b, c**).

The evidence of a functional link between Vav2 and Ret suggests that the two proteins may function together in a complex to regulate limbic DAT activity. Yeast two-hybrid (Y2H) assay revealed that Vav2 bound to intracellular domain (ICD) of Ret, whereas Vav3 interacted much more weakly with Ret ICD than Vav2 in yeast cells (**Fig. 3f** and **Supplementary Fig. 4a)**. Co-IP assay confirmed that there was no interaction between Vav3 and full-length Ret in HEK293 cells (**Supplementary Fig. 4b**). Moreover, a fragment of Vav2 that mediates the interaction between Vav2 and Ret was identified. Among a series of deletion mutants of Vav2, C-terminal SH2 domain of Vav2 was the minimal fragment for direct interaction between Vav2 and Ret (**Fig. 3f**). Glutathione S-transferase (GST) pull-down or co-IP assay confirmed the observation that Vav2, through its adaptor domain, interacted with the phosphorylated

full-length Ret (**Fig. 3g, h**). Ret also co-immunoprecipitated with Vav2 in VTA tissue lysates from adult mouse brain (**Fig. 6f**). Moreover, the binding between full-length Ret and Vav2 (**Fig. 3h**) or Vav2 adaptor domain (**Fig. 3g**) was in a Ret phosphorylation(s)-dependent manner, because inhibition of Ret kinase using the inhibitor 4-amino-5-(4-chlorophenyl)-7-(t-butyl)pyrazolo[3,4- d]pyramidine (PP2), but not its negative control 4-amino-7-phenylpyrazolo[3,4-d]pyramidine (PP3)[32], drastically suppressed the phosphorylation of Vav2 and the interaction between phospho-Vav2 and phospho-Ret in HEK293 cells (**Fig. 3h**). Similarly, co-expression of Vav2 and Ret resulted in enhanced phosphorylation of Vav2 tyrosine residue(s), which was also abrogated by PP2 only (**Fig. 3h**).

Tyrosine phosphorylation of Ret is crucial for activation of downstream signaling[31]. We next sought to identify the tyrosine residues of Ret that are responsible for Vav2 activation by using Y2H assay. Each of the sixteen tyrosine residues in Ret ICD, which have been reported to be phosphorylation sites following GDNF stimulation[33], was replaced with phenylalanine individually. Of the sixteen Ret mutants examined, only Y905F mutant lacking intrinsic kinase activity failed to interact with Vav2 (**Fig. 3i**). GST pull-down and co-IP assays confirmed that mutation in Y905F dramatically abolished Ret binding to Vav2 (**Fig. 3j, k**), suggesting that Vav2 interacts specifically with the GDNF-activated form of the Ret. Taken together, these data suggest that Vav2 binds with phosphorylated Ret and is a substrate of Ret receptor tyrosine kinase.

Vav2 is recruited into GDNF/Ret signaling to regulate DAT function

Next, we evaluated the impact of Ret/Vav2 signaling on the modulation of DAT function. To investigate whether Vav2 is required for Ret-mediated DAT regulation, shRNA-mediated Vav2 knockdown was performed in HEK293 cell line stably expressing YFP-DAT. Ret overexpression-induced suppression of DA uptake was markedly relieved by shRNA-mediated knockdown of Vav2 (**Fig. 4a**). In contrast, TrkA, a tyrosine receptor kinase, which was reported to activate Vav1 in immune systems[34], did not significantly alter DAT transporter activity (**Supplementary Fig. 4e).**

We then determined whether GDNF functions via Ret/Vav2 signaling to directly regulate DAT activity. Exposure of human neuroblastoma SH-SY5Y cell line, which expresses GDNF receptors and Vav2, to GDNF increased Vav2 tyrosine phosphorylation(s) and promoted Ret-Vav2 interaction (**Fig. 4b-c**), suggesting the Ret/Vav2 signaling is biochemically activated by GDNF. Augmentation of GDNF/Ret signaling by treatment of N2a cell line stably expressing RFP-tagged human DAT and GDNF co-receptor GFRα1 with GDNF resulted in a marked reduction in the levels of DA uptake as revealed in [^{3}H]DA uptake assay (**Fig. 4d**), suggesting that GDNF is a regulator for DAT activity, echoing previous study demonstrating higher DAT activity in *GDNF*$^{+/-}$ mice[30]. Treatment of these cells with GDNF also resulted in elevated Tyr905 phosphorylation of endogenous Ret (**Supplementary Fig. 4c)**, leading to decreased surface expression of Ret and DAT, but not total DAT levels which was accompanied by decreased DA uptake (**Fig. 4e, f, Supplementary Fig. 8e**). **Notably, GDNF induced a much larger change in DAT surface levels than DAT activity, suggesting that biotinylated DAT partially overlapped with functional DAT.** Moreover, the

GDNF-induced suppression of DAT transporter activity and DAT surface expression, but not total DAT levels, were markedly attenuated by shRNA knockdown of Vav2 (**Fig. 4g**, **h**, **Supplementary Fig. 8f**).

PKC is known as an important regulator for DAT trafficking and activity. We thus investigated the potential association between the GDNF signaling and PKC-mediated DAT regulation. We examined the role of Vav2 on the PKC-mediated down-regulation of DAT activity. In HEK293 cells, Vav2 knock-down partially blocked PKC activator phorbol 12-myristate 13-acetate (PMA)-induced reduction in DA uptake (**Supplementary Fig. 5a**), although the GDNF-induced down-regulation of DAT transporter activity in the N2a cells was not significantly attenuated by pretreatment of PKC inhibitor GF109203X (**Supplementary Fig. 5b)**, suggesting that Vav2 may be functionally associated with PKC' action on DAT regulation. These results collectively suggest that Vav2 participates in the GDNF signaling to negatively regulate DAT function. There is a potential functional interaction between GDNF/Ret/Vav2 signaling and PKC signaling in the context of DAT regulation.

Binding between Ret and DAT is required for Ret-DAT co-internalization

Given that Vav2 was immunoprecipitated with DAT and Ret individually (**Figs. 2, 3**), we speculated that Ret may interact with DAT in plasma membrane, provides a molecular basis for their co-internalization. Toward this end, we analyzed the potential interaction between Ret and DAT using split-ubiquitin membrane-based yeast-two-hybrid assay. Colony growth assay on the SD-His medium showed the DAT-Cub-LexA-VP16 and Ret-NubG were

expressed with no self-activation of the histidine reporter gene expression (**Supplementary Fig. 6a**). Hence, we used the system to determine whether the two membrane proteins bind to each other. It was revealed that DAT interacted with Ret (**Fig. 5a**), **providing evidence consistent with a direct interaction.** This result was confirmed by co-IP assay using tissue lysates from the NAc and dSTR (**Fig. 5b, c**) as well as immunocytochemical staining showing co-localization of DAT and Ret in primary cultured mesencephalic neurons (**Fig. 5d**). We also found that the binding between Ret and DAT was independent of Ret phosphorylation status, as evidenced by the fact that PP2 treatment had no significant impact on the interaction between Ret and DAT in HEK293 cells (**Supplementary Fig. 6b**), suggesting the Ret-DAT binding assumes different nature from Ret-Vav2 interaction, in which the phosphorylation of Ret is absolutely required (**Fig. 2**). Also, co-expression of Ret and hDAT in HEK293 cells did no significantly alter Thr^{53} phosphorylation levels of DAT (**Supplementary Fig. 6c**). These results further support the observation that GDNF/Ret/Vav2 signaling is vital for the regulation of DAT trafficking.

Vav2 is required for DAT trafficking in the context of cocaine

Previous studies have demonstrated that acute cocaine administration in rodents leads to elevated surface DAT expression and DAT activity[35, 36]. Hence we examined whether Vav2 is involved in the regulation of DAT expression in response to cocaine. As expected, acute administration of cocaine resulted in a significant increase in levels of cell-surface, but not total, DAT expression in both the NAc and dSTR synaptosomes of WT mice compared with saline-treated control (**Fig. 6a-c, Supplementary Fig. 8g**, **h**). This may be partially explained

by impaired Ret/Vav2 signaling, as manifested by marked decreases in the binding between Vav2 and Ret (**Fig. 6f**), which may allow more DAT protein released from the Ret/Vav2/DAT complex for its membrane accumulation. Comparatively, increased DAT surface expression was seen in the NAc, but not dSTR, of saline-treated *Vav2* KO mice. However, there was a dramatic decrease in the DAT surface expression and a trend toward the decrease in the of extracellular DA levels in the NAc of *Vav2* KO mice administrated with cocaine compared with cocaine-treated WT mice (**Fig. 6a-c** and **Supplementary Fig. 7d**), indicating that dysfunction of Vav2 contributes to cocaine-induced an abnormal distribution of limbic surface DATs and cleft DA levels. Notably, a similar trend for the DAT activity was also found in cocaine-treated *Vav2*-null mice (**Fig. 6d-e**). Furthermore, the cocaine-induced tissue DA increases in the NAc of WT mice was blocked in *Vav2* KO mice (**Fig. 6g**), indicating that the DAT in *Vav2* KO mice failed to functionally response to cocaine stimulation. In contrast, *Vav3*$^{-/-}$ mice and their WT counterparts displayed similar tissue DA levels following cocaine administration (**Fig. 6h**). These results suggest that cocaine exposure impairs the Ret/Vav2 signaling pathway leading to dysregulated DAT function and unbalanced DA homeostasis in limbic DA neuron terminals.

Loss of Vav2 attenuates cocaine-induced addictive behaviors

To assess the impact of Vav2-mediated DAT trafficking in the context of cocaine-induced addiction, we examined a series of behaviors in *Vav2*$^{-/-}$ mice and controls. Monitoring spontaneous activity, *Vav2*$^{-/-}$ animals showed no significant difference in either novelty-associated locomotion over 30 min or in total locomotor activity patterns over the

following 24 h when placed in a novel environment (**Fig. 7a** and **Supplementary Fig. 7a**). Cocaine administered daily produced the expected increase in locomotor activity, and the magnitude of the response was larger on day 16 than on day 1, indicating the development of behavioral sensitization (**Fig. 7b**). However, *Vav2*, but not *Vav3*, KO response was significantly blunted on day 3 onwards compared to WT mice following cocaine administration (**Fig. 7b, c**). Consistent with these results, *Vav2*$^{-/-}$ mice administrated with nomifensine, a specific DAT inhibitor, showed reduced and delayed locomotor activity (**Supplementary Fig. 7b, c**). The extracellular DA concentrations did not differ significantly between genotypes, but a trend toward decrease levels was seen in the NAc of *Vav2*$^{-/-}$ mice exposed to cocaine compared with WT mice as indicated in microdialysis (**Supplementary Fig. 7d**). Moreover, the conditional place preference (CPP) test revealed that no preference evoked by low dose of cocaine (5 mg/kg) or significantly decreased preference (10 mg/kg cocaine) for the compartment paired with cocaine in *Vav2*$^{-/-}$, whereas different doses of cocaine (5, 10 mg/kg) induced robust CPP in WT mice (**Fig. 7d**). This was not due to impaired learning and memory, or a difference in the basal CPP, because there was no significant difference in performance in the sucrose preference and contextual fear-conditioning between genotypes (**Fig. 7g, h**). In comparison, *Vav3*$^{-/-}$ mice did not display significant change in CPP assay compared with WT control (**Fig. 7f**). *Vav2*$^{-/-}$ mice also exhibited normal response to the acoustic startle stimulation and prepulse inhibition (**Supplementary Fig. 7e, f**). Notably, the attenuated cocaine-induced CPP in *Vav2*-deficient mice can be rescued by adeno-associated virus (AAV)-mediated Vav2 gene transfection selectively in the VTA (**Fig. 7d**), strongly suggesting that Vav2, particularly the ones

expressed in the VTA, is a mediator for the development of cocaine-induced addictive behaviors. This notion is further supported by the observation that the DAT activities, which was accompanied with the CPP scores, in the rescued mice were also restored to control levels, (**Fig. 7d, e**). Taken together, cocaine-induced addictive behaviors are attenuated in *Vav2*-null mice and there is a correlation between the behavioral responses and DAT activity in these animals. **Because flucturating levels of 5-HT may affect behavioral measures made with these mice, the contribution of the elevation of 5-HT levels, although small, in *Vav2*-null mice to these behavioral changes needs to be determined in future study.**

Discussion

Despite importance of DAT under both the physiological and pathological conditions, little is known about how DAT trafficking is regulated *in vivo* and the functional contribution of these mechanisms to the maintenance of DA homeostasis in single DA neuron terminals in brain. The present study demonstrates that *Vav2*-deficiency caused an abnormal increase in intracellular DA levels preferentially in the NAc, largely due to DAT hyper-function. *Vav2*$^{-/-}$ mice showed reduced behavioral response to cocaine. Moreover, Vav2 interacts with Ret forming a functional complex and cooperates to robustly down-regulate DAT activity. These data confirmed that Vav2-mediated DAT sequestration machinery plays a key role in the maintenance of DA homeostasis of DA neuron terminals in a brain region that is critical component of the neural circuitry involved in drug addiction.

Vav2 regulates DA homeostasis of mesolimbic DA neuron terminals in a regional-specific manner

We showed that the function of Vav2 on the regulation of DA homeostasis is specific to the mesolimbic system, as evidenced by the fact that Vav2 is a VTA-enriched protein in adult mouse brain and *Vav2*- or *Ret*-deficiency caused increases in the levels of DA selectively in the NAc. However, in agreement with previous studies by others[37], the striatal DA levels were not perturbed in Ret$^{+/-}$ mice. Overexpression of Vav2 in the VTA attenuated *Ret*-deficiency-induced DAT hyperfunction, demonstrating a causal relationship between the membrane DAT expression and Vav2 activation. These data thus provide a regulatory mechanism for the exquisite specificity of regulation of limbic DA homeostasis.

VTA DA neurons have some uniqueness in molecular characteristics over its adjacent nucleus SN. Previous studies have identified a few proteins that preferentially expressed in the VTA, such as calbindin-D28K[38], Otx2[39], play important roles in various activities. However, none of them has been linked with the regulation of DA homeostasis. GPR37, a negative regulator on DAT trafficking, is reported to have converse effect on vesicle DA storage in the striatum but not the NAc[40], supporting the notion of molecular difference between the NAc and dSTR on DAT regulation[41]. Thus, to the best of our knowledge, Vav2 is the first protein identified that is preferentially expressed in the VTA DA neurons and regulates DA homeostasis in mesolimbic DA neuron terminals *in vivo* via the modulation of DAT.

The question is, however, whether the somal Vav2 translates its function into the terminal thereby regulating NAc DAT activity, given the higher protein level of Vav2 in the VTA relative to NAc. Previous studies showed that Vav2 exhibits a ubiquitous pattern of expression[10, 42]. Vav2 colocalizes with synaptic proteins or proteins that are associated with synapses, including N-cadherin, p120ctn and filamentous actin in the hippocampus or cultured hippocampal neurons[11, 43], implying that Vav2 functions in nerve terminals. It is thus conceivable that Vav2 works together with Ret in the nerve terminal propagating GDNF retrograde signals[44]. There is evidence that Ret is expressed in the soma of the VAT dopaminergic neurons[37]. Together with the findings by Pickel and colleagues [45-47], it is very likely that Vav2 also function in the cell body with Ret and DAT.

Previous studies suggest that Vav2 and Vav3 perform a similar function in many different occasions[10, 48]. However, we found in the present study that Vav2 played distinct roles from Vav3 in the modulation of DA homeostasis in DA neuron terminals. In the brain, loss of *Vav2*, but not *Vav3*, resulted in marked elevation of intracellular DA levels (**Fig. 1**). In contrast, in the peripheral sympathetic nervous system, deficiency of *Vav3* or *Vav2*, causes significant perturbations in the concentration of plasma catecholamines[18, 19]. These data demonstrate intriguing specialization of Vav family members in the nervous system. Vav2 and Vav3 regulate the catecholamine levels of the central and peripheral nervous systems in a complimentary manner, representing two mechanistically distinct molecular pathways used in the regulation of DA homeostasis at DA neuron terminals.

GDNF/Ret/Vav2 is a novel signaling cascade that regulates DAT trafficking and DA homeostasis in DA neuron terminals

The present findings suggest a novel mechanism of DAT functional regulation via Ret/Vav2 activation evoked by GDNF. Vav2 is considered to be involved in the RTK signaling regulation of cell differentiation and outgrowth during brain development[10, 11]. Activation of RTK would normally cause the receptor itself down-regulated by phosphorylation and internalization, thus terminating the signal of the growth factor[10, 16]. We found in the present study that Vav2 mediated concomitant internalization of both DAT and RTK in response to GDNF treatment. The binding between DAT and Ret is requisite for their co-internalization. This finding is in agreement with previous findings that both Ret and DAT are localized in membrane microdomain (also known as lipid rafts)[49, 50]. How might Vav2

modulate DAT function? A likely scenario is that tight binding between DAT and Ret allows their redistribution from the cell plasma membrane domains into endosomes. During this process, Vav2 was phosphorylated and subsequently recruited to the Ret-DAT complex through interacting with phosphorylated Ret on residue Tyr905. Vav2 then may activate Rho small GTPase by catalysing the exchange of GDP for GTP contributing to endocytosis. Thus, Vav2 functions herein in the way that is distinct from those shown in previous studies, where Vav2 is shown to mediates internalization of RTKs themselves (e.g. Eph, TrkB) alone contributing to brain development[10, 51]. Moreover, it was shown that activation of PKC induced the internalization of DAT into early and recycling endosomes containing Rab5[52]. In contrast, in our study, activation of Ret/Vav2 signaling resulted in the internalization of DAT, suggesting differential regulation of DAT in distinct contexts. Altogether, our findings reveal a previously unrecognized role of Ret/Vav2 signaling in regulating DAT membrane expression and DA homeostasis in DA neuron terminals (**Fig. 7i**). It is likely that DAT is internalized through different signaling pathways, leading to distinct final destinations.

Role of Vav2 in the constitutive trafficking of DAT

It is well established that plasma membrane DAT undergoes both constitutive and substrate-mediated trafficking[53-55]. Our study demonstrated that in both non-neural cell HEK293 and neuronal cell N2a cells, Vav2 was both necessary and sufficient to promote constitutive DAT trafficking. Vav2 is thus identified as a novel regulator of constitutive DAT trafficking, highlighting its essential role in DAT regulation and DA homeostasis.

Our data also suggest that Vav2 participates in the GDNF-mediated DAT internalization which alters its function. Numerous studies have demonstrated that PKC-mediated DAT trafficking plays significant roles on the DAT activity[2, 55, 56]. Our study suggest that Vav2 is involved in PKC-regulated DAT trafficking, as shRNA knock-down of Vav2 in HEK293 cells partially blocked the PMA-induced down-regulation of DA uptake. Meanwhile, the GDNF-induced down-regulations of DA uptake was partially hindered by pretreatment of N2a cell line with a PKC inhibitor. One possible explanation for the interaction between Ret/Vav2 signaling and PKC is that among the downstream cascades of GDNF signaling, PKC represents one of effectors activated in response to GDNF/Ret[57]. Further study may be required for understanding the cross-talk between PKC and GDNF/Ret/Vav2 signaling.

Role of Vav2 in cocaine-induced DAT surface expression

It has been widely accepted that psychostimulants and natural rewards have the mesolimbic DA system as a common substrate. However, the underlying mechanisms are poorly understood. Our findings that the elevation of DA levels was unique to the NAc and not seen in the dSTR in *Vav2* KO mice, suggest that the reduced responses to cocaine as well as diminished cocaine place conditioning were due to the deficits in the mesolimbic DA pathway. Moreover, it is interesting that cocaine dramatically increases DAT surface expression in mammals[35, 58], although the underlying molecular mechanisms remain elusive. There are two ways Vav2 may contribute to this process. First, the significant reduction evoked by cocaine in the binding between Ret and Vav2 suggests the impairment of Ret/Vav2 signaling, which may allow more DAT protein released from the Ret/Vav2 complex within the

tubulovesicular structure for its membrane accumulation. Second, Vav2 may be required for DAT recycling from the endosomic recycling pool to the cell surface in the context of cocaine, but not under normal conditions, since there was a dramatic reduction of cell-surface DAT in the NAc of *Vav2*-null mice following acute cocaine treatment (**Fig. 6**). These results indicate that Vav2 is an important player in the signaling pathways in response to cocaine. Our study thus provide a potentially new avenue for the development of anti-addiction therapeutics based on the Vav2-mediated modulation of DAT trafficking.

Correlation between Vav2-regulated DAT surface expression and behavioral response to cocaine

How a loss of Vav2 function contributes to the reduced addictive behavior of *Vav2*-null mice? It has been shown that cocaine targets DAT and enhances its membrane surface expression[59], possibly by inserting DATs from the endosomic recycling pool into the plasma membrane[60]. Following cocaine's significant initial inhibition of the DAT and increase in extracellular DA levels in rodents, NAc DAT function may be rapidly up-regulated to compensate for the initial inhibition. Indeed, the acute *in vivo* exposure to cocaine markedly up-regulate DAT function and tissue DA levels (mainly reflects DA contents in synaptosomes) selectively in the NAc (**Fig. 6d, g**), which is in accordance with previous studies showing acute *in vivo* exposure to higher dose cocaine can rapidly and markedly up-regulate DAT function in synaptosomes prepared from rat NAc[36]. Importantly, the ability to rapidly up-regulate DAT function in response to acute cocaine is highly correlated with cocaine-induced locomotion[61]. In the present study, following acute exposure to cocaine,

Vav2-null mice showed reduced DAT activity and surface expression in the NAc which markedly compromised their ability to rapidly elevate DAT function and ultimately contribute to their lower cocaine-induced locomotor activation. This is supported by the finding that cocaine-treated wild-type mice exhibited greater extracellular DA levels than cocaine-treated *Vav2*-null mice (**Supplementary Fig. 7**). Moreover, the poor performance of *Vav2*-null mice in the CPP test was rescued by Vav2 overexpression which was accompanied with enhanced DAT activity (**Fig. 7d, e**). Thus, the present study strongly suggests that Vav2-mediated regulation of DAT surface expression and activity is correlated with controlling of behavioral effects of the acute cocaine.

METHODS

Methods and any associated references are available in the Supplementary information.

ACKNOWLEDGEMENTS

We thank Drs. XC Zhen for providing the DAT cDNA; C He for human Ret; HL Hu and ZL Qiu for the AAV virus constructs; LP Cheng for the *Ret* mutant mice; K Kobayashi for the TH-GFP transgenic mice. We also thank the Optical Imaging Center of ION for technical support in confocal microscopy; the Behavioral Core of ION for providing facilities and assistance. This work was supported by grants from the National Key Basic Research Program of China (2015CB553500, 2011CB504102), Natural Science Foundation of China (31123002, 31321091 and 30621130075), Beijing Institute for Brain Disorders (BIBD-PXM2013_014226_07_000084) and the Strategic Priority Research Program (B) of

Chinese Academy of Sciences (XDB01020300). XRB work has been funded by the Spanish Ministry of Economy and Competitiveness (SAF2009-07172, SAF2012-3171, RD06/0020/0001 and RD12/0036/0002), the Castilla-León Autonomous Government (CSI101U13) and Asociación Española Contra el Cáncer (AECC).

AUTHOR CONTRIBUTIONS

S.-y.Z. conducted most of the biochemical experiments and the data analysis, C.-j.Z. conducted most of the in vivo experiments and the data analysis. Y.-y.W. conducted some of the in vivo and in vitro experiments. Q.-q.Y contributed to the *in vitro* experiments. A.-y.S. and J.-f.W. contributed to mutant and protein interaction analysis. T.-p.W. contributes to CPP assay. Y.-q.Y. conducted in situ hybridization; Y.-q.Y., Y.-d.L. and J.-c.H. conducted genotyping; X.-h.Z contributes to *in vitro* experiments. X.-s.G., G.-m.Z., and X.-m.W. provided advice; X.R.B. provided *Vav2/3*-null mice, Vav2/3 constructs and J.-w.Z. supervised the project and wrote the manuscript.

COMPETING FINANCIAL INTERESTS

The authors declare no competing financial interests.

REFERENCES

1. Jones, S.R.*, et al.* Profound neuronal plasticity in response to inactivation of the dopamine transporter. *Proc Natl Acad Sci U S A* **95**, 4029-4034 (1998).

2. Loder, M.K. & Melikian, H.E. The dopamine transporter constitutively internalizes and recycles in a protein kinase C-regulated manner in stably transfected PC12 cell lines. *J Biol Chem* **278**, 22168-22174 (2003).

3. Gabriel, L.R.*, et al.* Dopamine transporter endocytic trafficking in striatal dopaminergic neurons: differential dependence on dynamin and the actin cytoskeleton. *J Neurosci* **33**, 17836-17846 (2013).

4. Holton, K.L., Loder, M.K. & Melikian, H.E. Nonclassical, distinct endocytic signals dictate constitutive and PKC-regulated neurotransmitter transporter internalization. *Nat Neurosci* **8**, 881-888 (2005).

5. Torres, G.E.*, et al.* Functional interaction between monoamine plasma membrane transporters and the synaptic PDZ domain-containing protein PICK1. *Neuron* **30**, 121-134 (2001).

6. Carneiro, A.M.*, et al.* The multiple LIM domain-containing adaptor protein Hic-5 synaptically colocalizes and interacts with the dopamine transporter. *J Neurosci* **22**, 7045-7054 (2002).

7. Fog, J.U.*, et al.* Calmodulin kinase II interacts with the dopamine transporter C terminus to regulate amphetamine-induced reverse transport. *Neuron* **51**, 417-429 (2006).

8. Cremona, M.L.*, et al.* Flotillin-1 is essential for PKC-triggered endocytosis and membrane microdomain localization of DAT. *Nat Neurosci* **14**, 469-477 (2011).

9. Navaroli, D.M., *et al.* The plasma membrane-associated GTPase Rin interacts with the dopamine transporter and is required for protein kinase C-regulated dopamine transporter trafficking. *J Neurosci* **31**, 13758-13770 (2011).

10. Cowan, C.W., *et al.* Vav family GEFs link activated Ephs to endocytosis and axon guidance. *Neuron* **46**, 205-217 (2005).

11. Hale, C.F., *et al.* Essential role for vav Guanine nucleotide exchange factors in brain-derived neurotrophic factor-induced dendritic spine growth and synapse plasticity. *J Neurosci* **31**, 12426-12436 (2011).

12. Schuebel, K.E., *et al.* Isolation and characterization of murine vav2, a member of the vav family of proto-oncogenes. *Oncogene* **13**, 363-371 (1996).

13. Movilla, N. & Bustelo, X.R. Biological and regulatory properties of Vav-3, a new member of the Vav family of oncoproteins. *Mol Cell Biol* **19**, 7870-7885 (1999).

14. Doody, G.M., *et al.* Signal transduction through Vav-2 participates in humoral immune responses and B cell maturation. *Nat Immunol* **2**, 542-547 (2001).

15. Quevedo, C., Sauzeau, V., Menacho-Marquez, M., Castro-Castro, A. & Bustelo, X.R. Vav3-deficient mice exhibit a transient delay in cerebellar development. *Mol Biol Cell* **21**, 1125-1139 (2010).

16. Bustelo, X.R., Ledbetter, J.A. & Barbacid, M. Product of vav proto-oncogene defines a new class of tyrosine protein kinase substrates. *Nature* **356**, 68-71 (1992).

17. Bustelo, X.R. Regulatory and signaling properties of the Vav family. *Mol Cell Biol* **20**, 1461-1477 (2000).

18. Sauzeau, V., Jerkic, M., Lopez-Novoa, J.M. & Bustelo, X.R. Loss of Vav2

proto-oncogene causes tachycardia and cardiovascular disease in mice. *Mol Biol Cell* **18**, 943-952 (2007).

19. Sauzeau, V.*, et al.* Vav3 proto-oncogene deficiency leads to sympathetic hyperactivity and cardiovascular dysfunction. *Nat Med* **12**, 841-845 (2006).

20. Matsushita, N.*, et al.* Dynamics of tyrosine hydroxylase promoter activity during midbrain dopaminergic neuron development. *J Neurochem* **82**, 295-304 (2002).

21. Best, J.A., Nijhout, H.F. & Reed, M.C. Homeostatic mechanisms in dopamine synthesis and release: a mathematical model. *Theoretical Biol Med Model* **6**, 21 (2009).

22. Kodama, A.*, et al.* Involvement of an SHP-2-Rho small G protein pathway in hepatocyte growth factor/scatter factor-induced cell scattering. *Mol Biol Cell* **11**, 2565-2575 (2000).

23. Vaughan, R.A., Huff, R.A., Uhl, G.R. & Kuhar, M.J. Protein kinase C-mediated phosphorylation and functional regulation of dopamine transporters in striatal synaptosomes. *J Biol Chem* **272**, 15541-15546 (1997).

24. Foster, J., Cervinski, M., Gorentla, B. & Vaughan, R. Regulation of the dopamine transporter by phosphorylation. in *Neurotransmitter Transporters* 197-214 (Springer, 2006).

25. Melikian, H.E. & Buckley, K.M. Membrane trafficking regulates the activity of the human dopamine transporter. *J Neurosci* **19**, 7699-7710 (1999).

26. Melikian, H.E. Neurotransmitter transporter trafficking: endocytosis, recycling, and regulation. *Pharmacol Ther* **104**, 17-27 (2004).

27. Daniels, G.M. & Amara, S.G. Regulated trafficking of the human dopamine transporter clathrin-mediated internalization and lysosomal degradation in response to phorbol esters. *J Biol Chem* **274**, 35794-35801 (1999).

28. Foster, J.D.*, et al.* Dopamine transporter phosphorylation site threonine 53 regulates substrate reuptake and amphetamine-stimulated efflux. *J Biol Chem* **287**, 29702-29712 (2012).

29. Yang, J.-W.*, et al.* Dopamine transporter phosphorylation site threonine 53 regulates substrate reuptake and amphetamine-stimulated efflux. *BMC Pharmacol Toxicol* **13**, A45 (2012).

30. Littrell, O.M.*, et al.* Enhanced dopamine transporter activity in middle-aged Gdnf heterozygous mice. *Neurobiol Aging* **33**, 427 e421-414 (2012).

31. Airaksinen, M.S. & Saarma, M. The GDNF family: signaling, biological functions and therapeutic value. *Nature Rev. Neurosci.* **3**, 383-394 (2002).

32. Vaughan, R.A., Huff, R.A., Uhl, G.R. & Kuhar, M.J. Protein kinase C-mediated phosphorylation and functional regulation of dopamine transporters in striatal synaptosomes. *J Biol Chem* **272**, 15541-15546 (1997).

33. Coulpier, M., Anders, J. & Ibanez, C.F. Coordinated activation of autophosphorylation sites in the RET receptor tyrosine kinase: importance of tyrosine 1062 for GDNF mediated neuronal differentiation and survival. *J Biol Chem* **277**, 1991-1999 (2002).

34. Melamed, I., Patel, H., Brodie, C. & Gelfand, E.W. Activation of Vav and Ras through the nerve growth factor and B cell receptors by different kinases. *Cell Immunol* **191**, 83-89 (1999).

35. Little, K.Y., Elmer, L.W., Zhong, H., Scheys, J.O. & Zhang, L. Cocaine induction of dopamine transporter trafficking to the plasma membrane. *Mol Pharmacol* **61**, 436-445 (2002).

36. Daws, L.C.*, et al.* Cocaine increases dopamine uptake and cell surface expression of dopamine transporters. *Biochem Biophys Res Commun* **290**, 1545-1550 (2002).

37. Jain, S.*, et al.* RET is dispensable for maintenance of midbrain dopaminergic neurons in adult mice. *J Neurosci* **26**, 11230-11238 (2006).

38. Liang, C.L., Sinton, C.M. & German, D.C. Midbrain dopaminergic neurons in the mouse: co-localization with Calbindin-D28K and calretinin. *Neuroscience* **75**, 523-533 (1996).

39. Di Salvio, M.*, et al.* Otx2 controls neuron subtype identity in ventral tegmental area and antagonizes vulnerability to MPTP. *Nat Neurosci* **13**, 1481-1488 (2010).

40. Marazziti, D.*, et al.* GPR37 associates with the dopamine transporter to modulate dopamine uptake and behavioral responses to dopaminergic drugs. *Proc Natl Acad Sci U S A* **104**, 9846-9851 (2007).

41. Glynn, G.E. & Yamamoto, B.K. In vivo neurochemical and anatomical heterogeneity of the dopamine uptake system in the rat caudate putamen. *Brain Res* **481**, 235-241 (1989).

42. Turner, M. & Billadeau, D.D. VAV proteins as signal integrators for multi-subunit immune-recognition receptors. *Nat Rev Immunol* **2**, 476-486 (2002).

43. Chauvet, N., Prieto, M., Fabre, C., Noren, N.K. & Privat, A. Distribution of p120 catenin during rat brain development: potential role in regulation of cadherin-mediated adhesion and actin cytoskeleton organization. *Mol Cell Neurosci* **22**, 467-486 (2003).

44. Coulpier, M. & Ibanez, C.F. Retrograde propagation of GDNF-mediated signals in sympathetic neurons. *Mol Cell Neurosci* **27**, 132-139 (2004).

45. Nirenberg, M.J.*, et al.* Immunogold localization of the dopamine transporter: an ultrastructural study of the rat ventral tegmental area. *J Neurosci* **17**, 5255-5262 (1997).

46. Nirenberg, M.J.*, et al.* Immunogold localization of the dopamine transporter: an ultrastructural study of the rat ventral tegmental area. *J Neurosci* **17**, 4037-4044 (1997).

47. Nirenberg, M.J., Vaughan, R.A., Uhl, G.R., Kuhar, M.J. & Pickel, V.M. The dopamine transporter is localized to dendritic and axonal plasma membranes of nigrostriatal dopaminergic neurons. *J Neurosci* **16**, 436-447 (1996).

48. Hunter, S.G.*, et al.* Essential role of Vav family guanine nucleotide exchange factors in EphA receptor-mediated angiogenesis. *Mol Cell Biol* **26**, 4830-4842 (2006).

49. Encinas, M.*, et al.* c-Src is required for glial cell line-derived neurotrophic factor (GDNF) family ligand-mediated neuronal survival via a phosphatidylinositol-3 kinase (PI-3K)-dependent pathway. *J Neurosci* **21**, 1464-1472 (2001).

50. Adkins, E.M.*, et al.* Membrane mobility and microdomain association of the dopamine transporter studied with fluorescence correlation spectroscopy and fluorescence recovery after photobleaching. *Biochemistry* **46**, 10484-10497 (2007).

51. Shamah, S.M.*, et al.* EphA receptors regulate growth cone dynamics through the novel guanine nucleotide exchange factor ephexin. *Cell* **105**, 233-244 (2001).

52. Sorkina, T., Hoover, B.R., Zahniser, N.R. & Sorkin, A. Constitutive and protein kinase C-induced internalization of the dopamine transporter is mediated by a clathrin-dependent mechanism. *Traffic* **6**, 157-170 (2005).

53. Loder, M.K. & Melikian, H.E. The dopamine transporter constitutively internalizes and recycles in a protein kinase C-regulated manner in stably transfected PC12 cell lines. *J Biol Chem* **278**, 22168-22174 (2003).

54. Kahlig, K.M. & Galli, A. Regulation of dopamine transporter function and plasma

membrane expression by dopamine, amphetamine, and cocaine. *Eur J Pharmacol* **479**, 153-158 (2003).

55. Melikian, H.E. Neurotransmitter transporter trafficking: endocytosis, recycling, and regulation. *Pharmacol Ther* **104**, 17-27 (2004).

56. Zahniser, N.R. & Sorkin, A. Trafficking of dopamine transporters in psychostimulant actions. *Semin Cell Dev Biol* **20**, 411-417 (2009).

57. Iwahashi, N., Murakami, H., Nimura, Y. & Takahashi, M. Activation of RET tyrosine kinase regulates interleukin-8 production by multiple signaling pathways. *Biochem Biophys Res Commun* **294**, 642-649 (2002).

58. Crits-Christoph, P.*, et al.* Dopamine transporter levels in cocaine dependent subjects. *Drug Alcohol Depend* **98**, 70-76 (2008).

59. Little, K.Y., Elmer, L.W., Zhong, H., Scheys, J.O. & Zhang, L. Cocaine induction of dopamine transporter trafficking to the plasma membrane. *Mol Pharmacol* **61**, 436-445 (2002).

60. Kahlig, K.M. & Galli, A. Regulation of dopamine transporter function and plasma membrane expression by dopamine, amphetamine, and cocaine. *Eur J Pharmacol* **479**, 153-158 (2003).

61. Mandt, B.H. & Zahniser, N.R. Low and high cocaine locomotor responding male Sprague-Dawley rats differ in rapid cocaine-induced regulation of striatal dopamine transporter function. *Neuropharmacology* **58**, 605-612 (2010).

Legends

Figure 1. Vav2 is a VTA-enriched protein that is required for DA homeostasis in the mesolimbic neuron terminals. (**a**) Immunoblotting reveals the Vav2 and TH levels in the olfactory bulb (OB), brain stem, nucleus accumbens (NAc), ventral tagmental area (VTA), substantia nigra (SN), dorsal striatum (dSTR), cerebrocortex, hippocampus and cerebellum in adult mouse brain. (**b**) Quantitative data shown in (**a**). (**c**) Immunoblotting reveals higher expression levels of Vav2 in the VTA of developing and adult TH-GFP transgenic mouse brain compared with the SN. (**d**) Quantitative data shown in (**c**). Data are expressed as mean ±S.E.M. (n=3~4 per group); Unpaired t-test, * $P<0.05$. (**e**) Immunoblotting reveals the Vav2 levels in the synpatosomes prepared from both the NAc and dSTR. DAT, a DA neuron marker serves as loading control. (**f**) Quantitative data shown in (**e**). (**g**) Vav2 *in situ* hybridization combined with TH immunohistochemistry reveals that Vav2 hybridization signals (purple) were localized in TH+ neurons (brown) in both the VTA (stippled box) and SN. Right panel is enlarged view from the stippled box. The insert is enlarged view from a box in the right panel. Arrow shows a typical cell with colocalization of Vav2 mRNA hybridization signals and TH immunoreactive signals. Scale bar, 200 μm. Data shown in (**a**-**f**) were from at least three independent experiments. (**h**) Double-labeled immunofluorescent staining shows that some TH+ (green) neurons co-express Vav2 (red) in the VTA and SNc of adult mouse brain (indicated with arrows). Right panel shows the enlarged view of stippled box in the left panel. Scale bar, 300 μm. (**i-n**) Measurement of catecholamine and their metabolites was performed in the NAc (**i-k**) and dSTR (**l-n**) of *Vav2* KO and WT mice. Data are expressed as mean±S.E.M. (n=14 per group); Unpaired t-test, * $P<0.05$.

Figure 2. Enhanced surface expression and DAT activity in *Vav2*-null mice. (**a**) Measurement of DAT transporter activities was performed in the synaptosomal preparations of NAc and dSTR of *Vav2*-null and wild-type mice. Data from three experiments are quantified. Data are expressed as mean±S.E.M. (n=3~4 per group); Unpaired t-test, **P*= 0.0026 <0.01. (**b**) Up-regulation of DAT activity in the NAc of *Vav2*-null mice was rescued by AAV-mediated Vav2 overexpression. Data are expressed as mean±S.E.M. (n=3~4 per group); Unpaired t-test, **P*= 0.0059 <0.01. (**c**) [^{3}H]DA uptake assessment was performed in the HEK293 cells transiently overexpressing small hairpin RNA specific to Vav2 (shVav2 #1) or a dominant negative form of Vav2 (Vav2 L212Q mutant). Data are expressed as mean±S.E.M. (n=3); Unpaired t-test, *P* = 0.0001 for shVav2 #1, *P*=0.0030 for L212Q, **P* <0.05. Inserts are immunoblot data showing the equal protein levels of β-actin between *Vav2*-RNAi and control. (**d**) [^{3}H]DA uptake assessment was performed in the N2a cells stably overexpressing RFP-tagged DAT and GFRα1. The cells were transfected with either shVav2 #1, #2 or Vav2 L212Q and maintained for 72 h before Western blotting analysis. Data are expressed as mean ±S.E.M. (n=3); One-way ANOVA.* *P*<0.05. Right panel is immunoblot data showing the equal protein levels of β-actin in each group. (**e**) [^{3}H]DA uptake assessment was performed in the N2a cells stably overexpressing RFP-DAT and GFRα1. The cells were transfected with shVav2 #2, RFP-tagged Vav2 or scrambled shRNA as control, respectively. Data are expressed as mean±S.E.M. (n=3); One way ANOVA, **P*=0.0246<0.05 for #2. (**f**) Surface biotinylation analysis shows the surface expression levels of DAT in the NAc and dSTR synaptosomal preparations in *Vav2*-null and WT mice. (**g**) Quantitative data shown in (**f**). Data are expressed as mean±S.E.M. (n=4); Unpaired t-test, **P*=0.0359<0.05 for NAc, **P*=0.2422<0.05 for dSTR (**h**, **i**) Surface biotinylation analysis to assess surface and total

DAT levels in HEK293 cells stably overexpressing YFP-tagged DAT. The cells were transiently transfected with shVav2 #2, RFP-tagged Vav2 or a constitutively active form of Vav2 (Vav2 Y172F mutant), respectively. (**j**) Kinetic characteristics of DAT-mediated DA uptake in the NAc synaptosomal preparations of *Vav2* KO and WT mice.

Figure 3. Vav2 is a substrate of Ret receptor tyrosine kinase contributing to the regulation of DAT trafficking and function. (**a**) [^{3}H]DA uptake assessment was performed in the NAc or dSTR synaptosomal preparations of $Ret^{+/-}$ mice and WT mice. Data are expressed as mean±S.E.M. (n=4); Unpaired t-test, **P*=0.0010<0.05 for NAc, *P*=0.8621 for dSTR. (**b**) Surface biotinylation combined with immunoblotting shows elevated levels of surface DAT in the NAc and dSTR synaptosomes of $Ret^{+/-}$ mice. (**c**) Quantitative data shown in (**b**). Data are expressed as mean±S.E.M. (n=3); Unpaired t-test, **P*=0.0323<0.05 for NAc, *P* =0.5316 for dSTR. (**d, e**) HPLC analysis of catecholamine and their metabolites in the NAc (**d**) and dSTR (**e**) of $Ret^{+/-}$ and WT mice. Data are expressed as mean±S.E.M. (n=7-9 per group); Unpaired t-test, **P*=0.0184<0.05 for DA. (**f**) Characterization of Vav2 and the intracellular domain of Ret interaction using yeast two-hybrid assay. GEF, guanine nucleotide exchange factor domain; SH2, Src homology 2 domain; SH3: Src homology 3 domain. (**g**) GST pull-down assay shows the interaction between Vav2 C-terminal fragment and Flag-tagged Ret which is abolished by PP2 (15 μM) treatment for 60 min before harvesting cells. (**h**) Co-IP reveals that Vav2 interacts with Ret in a kinase-dependent manner. PP2 or PP3 was added into cultures each at 15 μM for 60 min before cells were harvested. (**i**) Identification of the tyrosine residues of Ret that is responsible for Vav2 activation using site-directed mutagenesis combined with yeast two-hybridize assay. (**j, k**) GST pull-down (**j**) and co-IP (**k**) assays show

the GST-Vav2 C-terminal adaptor domain (GST-Vav2-C) interacts with Ret-Flag, but not Ret Y905F mutant. Data shown in (**f-h**, **j**, **k**) were from at least two independent experiments.

Figure 4. GDNF/Ret/Vav2 signaling modulates DAT activity. (**a**) [^{3}H]DA uptake assessment was performed in HEK293 cells overexpressing YFP-DAT which were transiently transfected with empty vector (Flag vector), Flag-tagged Ret, scrambled shRNA or shVav2 #1, respectively. Data are expressed as mean±S.E.M. (n=3); One-way ANOVA, P=0.0039<0.01 for Ret-Flag, P=0.0260<0.05 for Ret-Flag+scrambled shRNA, P> 0.9999 for Ret+shVav2 #1, * P<0.05. (**b**) GDNF stimulation (100 ng/ml) activates endogenous Vav2 in SH-SY5Y neuroblastoma cells. Cells were incubated with 100 ng/ml GDNF for various times. (**c**) GDNF treatment (100 ng/ml) enhances interaction between Vav2 and Ret in SH-SY5Y cells. Data are from two independent experiments. (**d**) [^{3}H]DA uptake assessment was performed in N2a cell line stably expressing RFP-tagged human DAT and GDNF co-receptor GFRα1 with GDNF (10, 100 ng/ml) for 30 min. Data are expressed as mean±S.E.M. (n=4). One-way ANOVA with Tukey's multiple comparison test, P=0.0061<0.01 for 10 mg/ml treatment groups, P<0.0001 for 100 mg/ml treatment groups, * P<0.05. (**e**) Surface biotinylation combined with immunoblotting shows decreases in the levels of surface Ret and DAT in N2a cells stably overexpressing RFP-DAT and GFRα1 following transient exposure to GDNF. (**f**) Quantitative data shown in (**e**). Data are expressed as mean±S.E.M. (n=4); Unpaired t-test, *P= 0.0014<0.05. (**g**, **h**) Surface biotinylation combined with immunoblotting and [^{3}H]DA uptake assessment shows decreases in the levels of surface DAT and DAT transporter activity in N2a cells stably overexpressing RFP-DAT and GFRα1 were abolished following

transfection with shVav2 #2. Data are expressed as mean±S.E.M. (n=3). Two-way ANOVA with Bonferroni's post test. *P*=0.0298 between control and GDNF in scramble group; *P* =0.9665 between control and GDNF in shVav2 group; *P* =0.0370 between scramble and shVav2 in control group, * *P*<0.05; n.s. no significance.

Figure 5. Ret interacts with DAT. (**a**) Split-ubiquitin membrane-based yeast two-hybridization assay shows that Ret interacts with DAT. Photographs show the growth of the transformants on SD(-Trp-Leu-His plus 3-AT at three different concentrations). (**b**, **c**) Co-IP shows that DAT interacts with Ret. (**d**) Immunofluorescent staining for DAT and Ret in the primary cultured mesencephalic neurons of E16 WT mouse embryos. Arrows indicate colocalization of immunosignals. Data are from at least two independent experiments. (**e**) Co-IP shows that interaction between Vav2 and DAT is enhanced in HEK293 cells stably overexpressing Flag-DAT-IRES-GFP with transient transfection of Ret.

Figure 6. Vav2 is required for DAT trafficking in the context of cocaine. (**a**) Surface biotinylation combined with immunoblotting reveals that acute cocaine (20 mg/kg) exposure induces significant alteration of surface expression of DAT in the synaptosomal preparations from the NAc of *Vav2* KO and WT mice. SAL, saline; COC, cocaine. (**b**, **c**) Quantitative data shown in (**a**). Data are expressed as mean±S.E.M. (n=3). Two-way ANOVA with Bonferroni's post test. * *P*<0.05; n.s. no significance. (**d, e**) [^{3}H]DA uptake assessment was performed in the synaptosomal preparations from the NAc (**d**) or dSTR (**e**) of *Vav2* KO and WT mice treated with either acute cocaine (20 mg/kg) or vehicle. Data are expressed as mean

±S.E.M. (NAc, n=3; dSTR, n=6-7); Two-way ANOVA followed by Bonferroni's multiple comparisons test. * $P<0.05$. n.s., no significance. (**f**) Co-IP assays show that cocaine (20 mg/kg) reduces binding between Ret and immuneprecipitated Vav2. Data are from at least two independent experiments. (**g**, **h**) Measurement of tissue DA levels from the NAc of either *Vav2* (**g**) or *Vav3* (**h**) KO and WT mice treated with saline or acute cocaine (20 mg/kg). Data are expressed as mean±S.E.M. (n=3). Two-way ANOVA followed by Bonferroni's post-hoc test, *$P<0.05$.

Figure 7. Altered cocaine-induced behavioral sensitization in *Vav2*-deficient mice. (**a**) The spontaneous activity of *Vav2* KO mice is not altered (n=17-18 per group). (**b**, **c**) The cocaine-induced behavioral sensitization of *Vav2* KO (n=12-16 per group) (**b**), but not *Vav3* KO (**c**) (n=8-10 per group), is altered compared with WT mice (Two-way ANOVA, $P<0.05$). * indicates that there is a significant difference ($P<0.05$) within subjects between the first and last days. (**d**, **e**) The performance in CPP test is assessed in *Vav2*-null and WT mice that received acute cocaine (5 or 10 mg/kg) and/or bilateral injection of AAV-GFP or AAV-Vav2 in the VTA (**d**). Two-way ANOVA with Sidak's post test. *$P=0.0031<0.05$ for KO vs WT treated with 5 mg/kg cocaine; *$P=0.0457<0.05$ for KO vs WT treated with 10 mg/kg cocaine; Data are expressed as mean±S.E.M. (n=8-12 per group). For AAV-transfected animals, unpaired t-test, $^{\#}P=0.0081<0.05$. Data are expressed as mean±S.E.M. (n=9 per group). (**e**) The DAT-mediated DA uptake of the animals examined in (**d**) was assessed after CPP test. (**f**) The performance in CPP is not significantly altered in *Vav3* KO mice (n=8 per group). (**g**) The performance in sucrose preference test is not altered in *Vav2* KO mice. Data are expressed as

mean±S.E.M. (n=9 per group). Unpaired t-test, *P*>0.05. (**h**) Recent memory of *Vav2* KO and WT mice is expressed as the percentage of time spent in freezing during contextual fear conditioning test. Data are expressed as mean±S.E.M. (n=16). Unpaired t-test, **P*<0.05. (**i**) A proposed model for how Vav2 regulates GDNF/Ret signaling thereby modulating DAT internalization and DA homeostasis in the mesolimbic DA neuron terminals of adult mice. **It is noted that cocaine could influence the trafficking of DAT in a way that intersects with RET/Vav2, given that the conformation of DAT when bound to cocaine disables the DAT/RET interaction, with no effect if Vav2 is absent. Moreover, elevated extracellular DA produced by cocaine acting normally to produce RET dephosphorylation and reduced Vav2 associations, and which is of no significance in the context of a Vav2 knockout.**

Figure 1

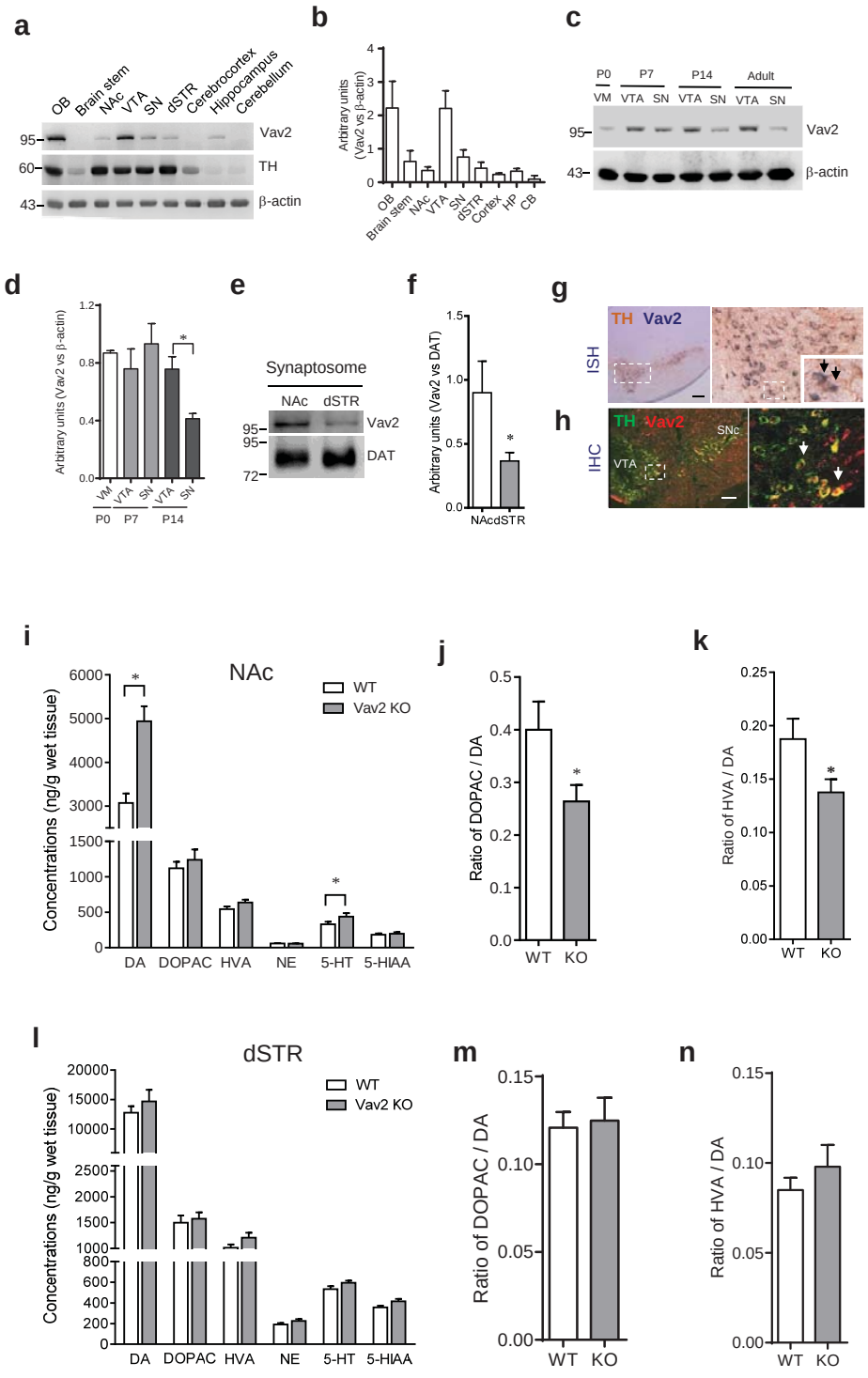
a
OB
Brain stem
NAc
VTA
SN
dSTR
Cerebrocortex
Hippocampus
Cerebellum
95
60
43
Vav2
TH
β-actin
b
Arbitrary units (Vav2 vs β-actin)
OB
Brain stem
NAc
VTA
SN
dSTR
Cortex
HP
CB
c
P0
P7
P14
Adult
VM
VTA
SN
95
43
Vav2
β-actin
d
Arbitrary units (Vav2 vs β-actin)
P0
P7
P14
e
Synaptosome
NAc
dSTR
95
95
72
Vav2
DAT
f
Arbitrary units (Vav2 vs DAT)
NAc
dSTR
g
ISH
TH
Vav2
h
IHC
TH
Vav2
SNc
VTA
i
NAc
WT
Vav2 KO
Concentrations (ng/g wet tissue)
DA
DOPAC
HVA
NE
5-HT
5-HIAA
j
Ratio of DOPAC / DA
WT
KO
k
Ratio of HVA / DA
WT
KO
l
dSTR
WT
Vav2 KO
Concentrations (ng/g wet tissue)
DA
DOPAC
HVA
NE
5-HT
5-HIAA
m
Ratio of DOPAC / DA
WT
KO
n
Ratio of HVA / DA
WT
KO

Figure 2

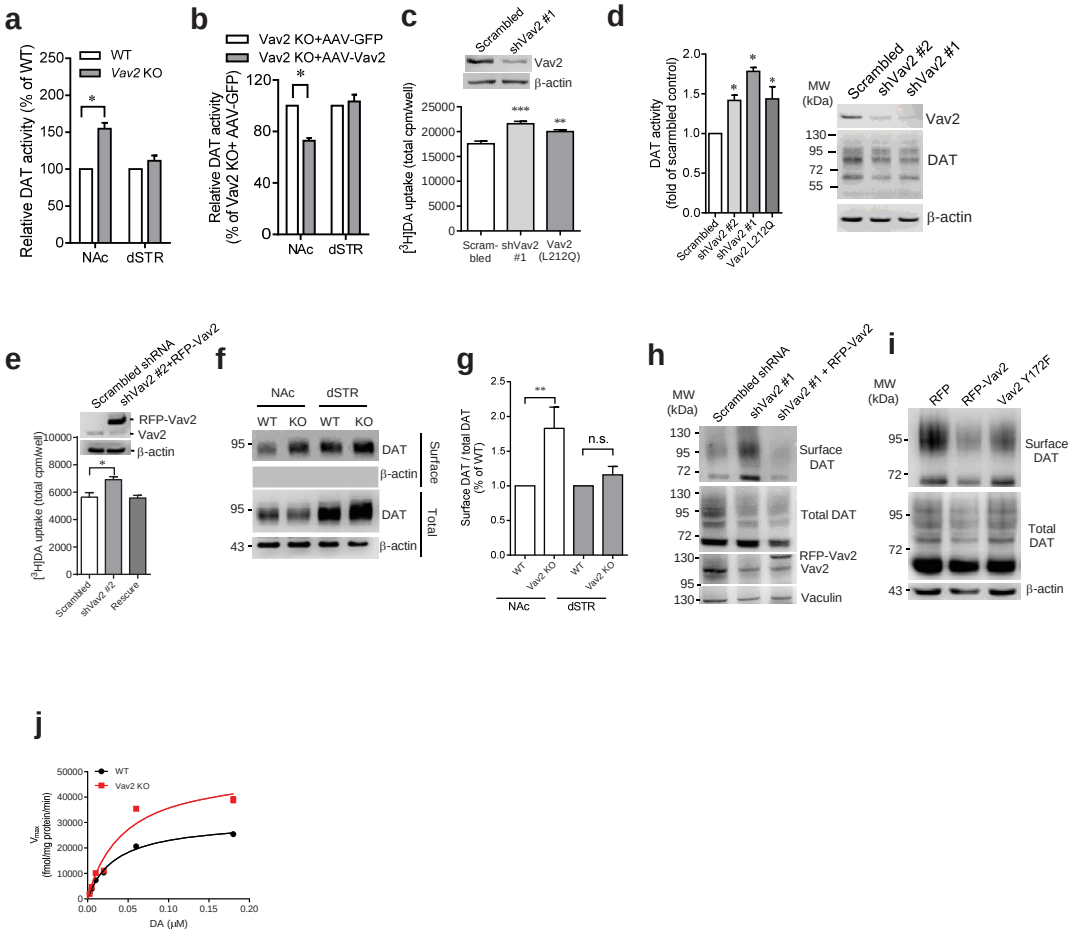
a
Relative DAT activity (% of WT)
WT
Vav2 KO
NAc
dSTR
b
Vav2 KO+AAV-GFP
Vav2 KO+AAV-Vav2
Relative DAT activity (% of Vav2 KO+ AAV-GFP)
c
Scrambled
shVav2 #1
Vav2
β-actin
[3H]DA uptake (total cpm/well)
Scram-bled
shVav2 #1
Vav2 (L212Q)
d
DAT activity (fold of scrambled control)
Scrambled
shVav2 #2
shVav2 #1
Vav2 L212Q
MW (kDa)
Vav2
DAT
β-actin
e
Scrambled shRNA
shVav2 #2+RFP-Vav2
RFP-Vav2
Vav2
β-actin
[3H]DA uptake (total cpm/well)
Rescue
f
NAc
dSTR
WT
KO
DAT
β-actin
Surface
Total
g
Surface DAT / total DAT (% of WT)
n.s.
h
shVav2 #1 + RFP-Vav2
Surface DAT
Total DAT
RFP-Vav2
Vav2
Vaculin
i
RFP
RFP-Vav2
Vav2 Y172F
Surface DAT
Total DAT
β-actin
j
WT
Vav2 KO
DA (μM)

Figure 3

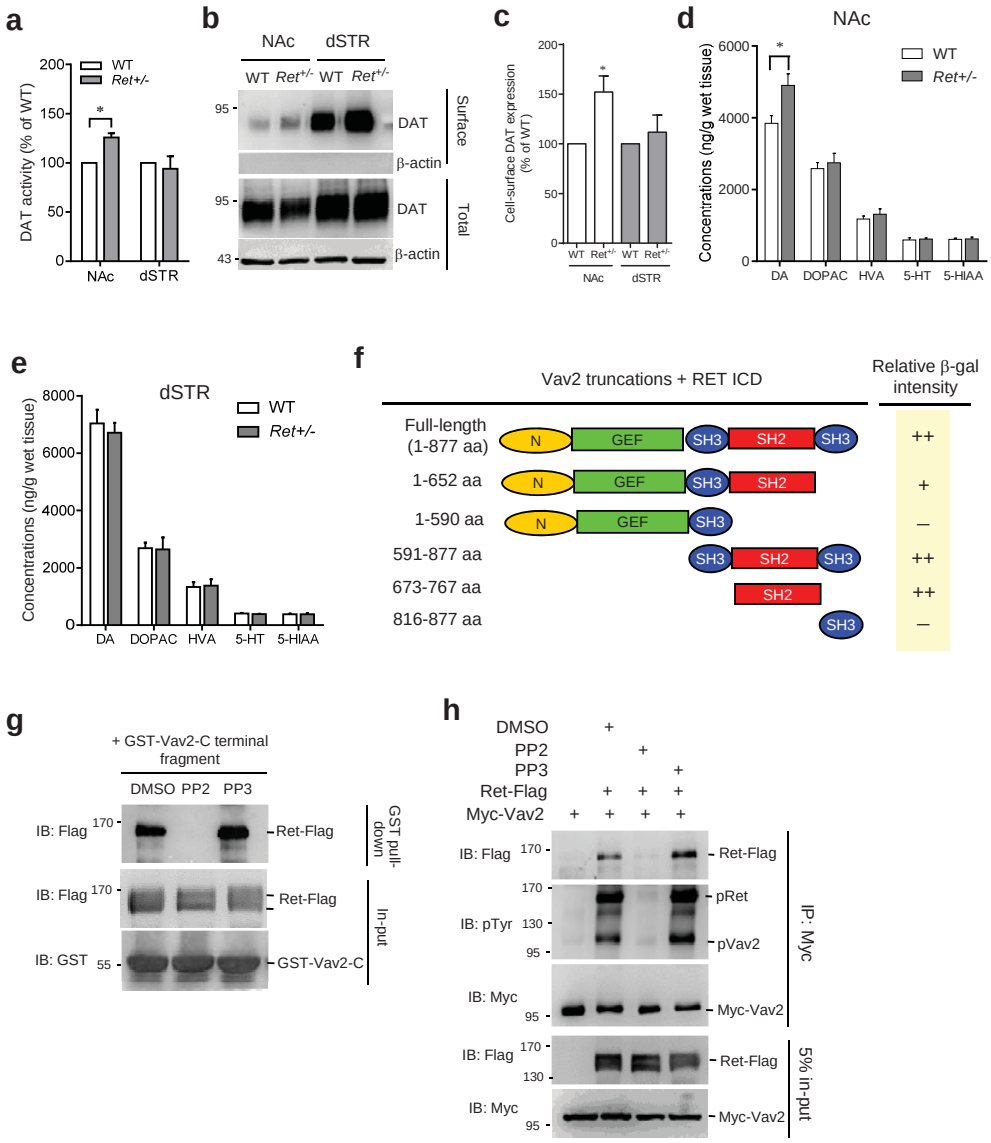
a
DAT activity (% of WT)
WT
Ret+/-
NAc
dSTR
b
NAc
dSTR
WT Ret+/- WT Ret+/-
DAT
β-actin
Surface
Total
c
Cell-surface DAT expression (% of WT)
d
NAc
Concentrations (ng/g wet tissue)
DA DOPAC HVA 5-HT 5-HIAA
e
dSTR
f
Vav2 truncations + RET ICD
Relative β-gal intensity
Full-length (1-877 aa)
1-652 aa
1-590 aa
591-877 aa
673-767 aa
816-877 aa
N
GEF
SH3
SH2
g
+ GST-Vav2-C terminal fragment
DMSO PP2 PP3
IB: Flag
Ret-Flag
GST pull-down
In-put
IB: GST
GST-Vav2-C
h
DMSO
PP2
PP3
Ret-Flag
Myc-Vav2
IB: pTyr
pRet
pVav2
IB: Myc
IP: Myc
5% In-put

Continued ..

i

AD \ BD	Y660F	Y687F	Y752F	Y791F	Y806F	Y809F	Y826F	Y864F	Y900F	Y905F	Y928F	Y952F	Y981F	Y1015F	Y1029F	Y1062F
Rel. β-gal intensity	+	+	+	+	+	+	+	+	+	—	+	+	+	+	+	+

j

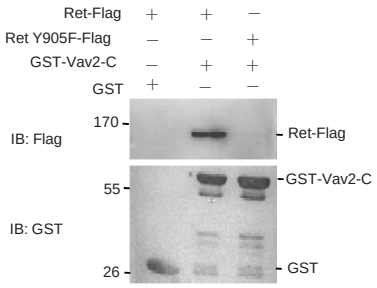

k

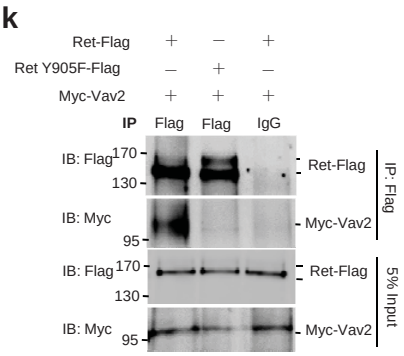

Figure 4

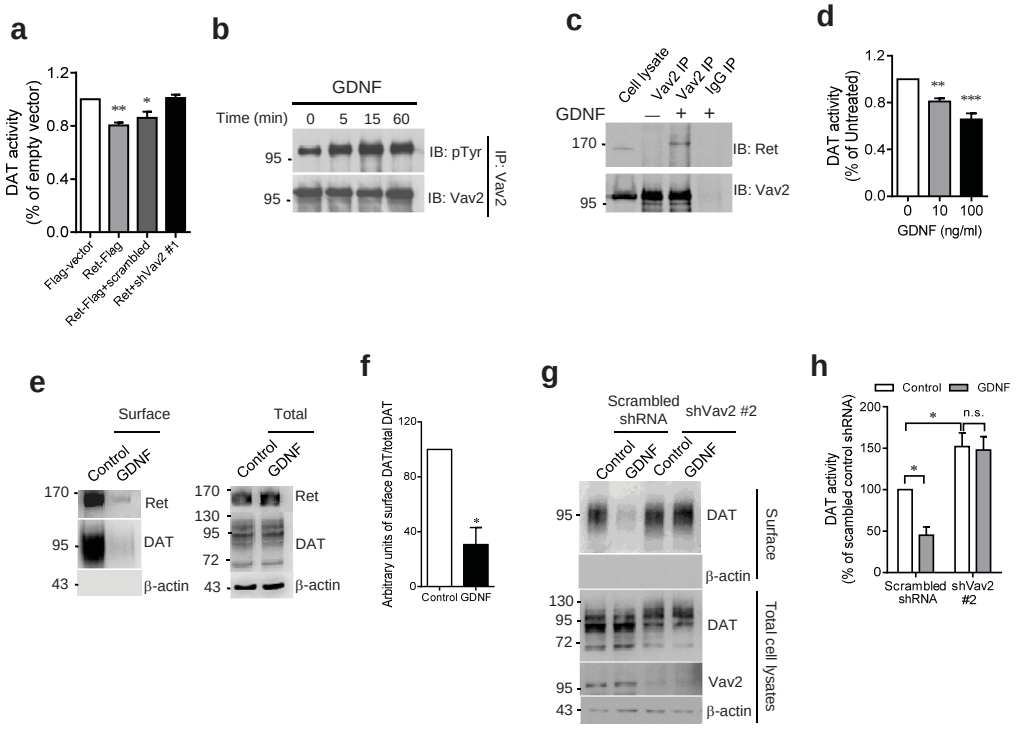
a
DAT activity (% of empty vector)
1.2
0.8
0.4
0.0
**
*
Flag-vector
Ret-Flag
Ret-Flag+scrambled
Ret+shVav2 #1
b
GDNF
Time (min) 0 5 15 60
95
95
IB: pTyr
IB: Vav2
IP: Vav2
c
Cell lysate
Vav2 IP
Vav2 IP
IgG IP
GDNF — + +
170
95
IB: Ret
IB: Vav2
d
DAT activity (% of Untreated)
1.2
0.8
0.4
0.0
**
***
0 10 100
GDNF (ng/ml)
e
Surface
Total
Control
GDNF
Control
GDNF
170
95
43
Ret
DAT
β-actin
170
130
95
72
43
Ret
DAT
β-actin
f
Arbitrary units of surface DAT/total DAT
120
80
40
0
*
Control GDNF
g
Scrambled shRNA
shVav2 #2
Control
GDNF
Control
GDNF
95
DAT
β-actin
Surface
130
95
72
DAT
Total cell lysates
95
Vav2
43
β-actin
h
Control
GDNF
DAT activity (% of scambled control shRNA)
200
150
100
50
0
*
n.s.
*
Scrambled shRNA
shVav2 #2

Figure 5

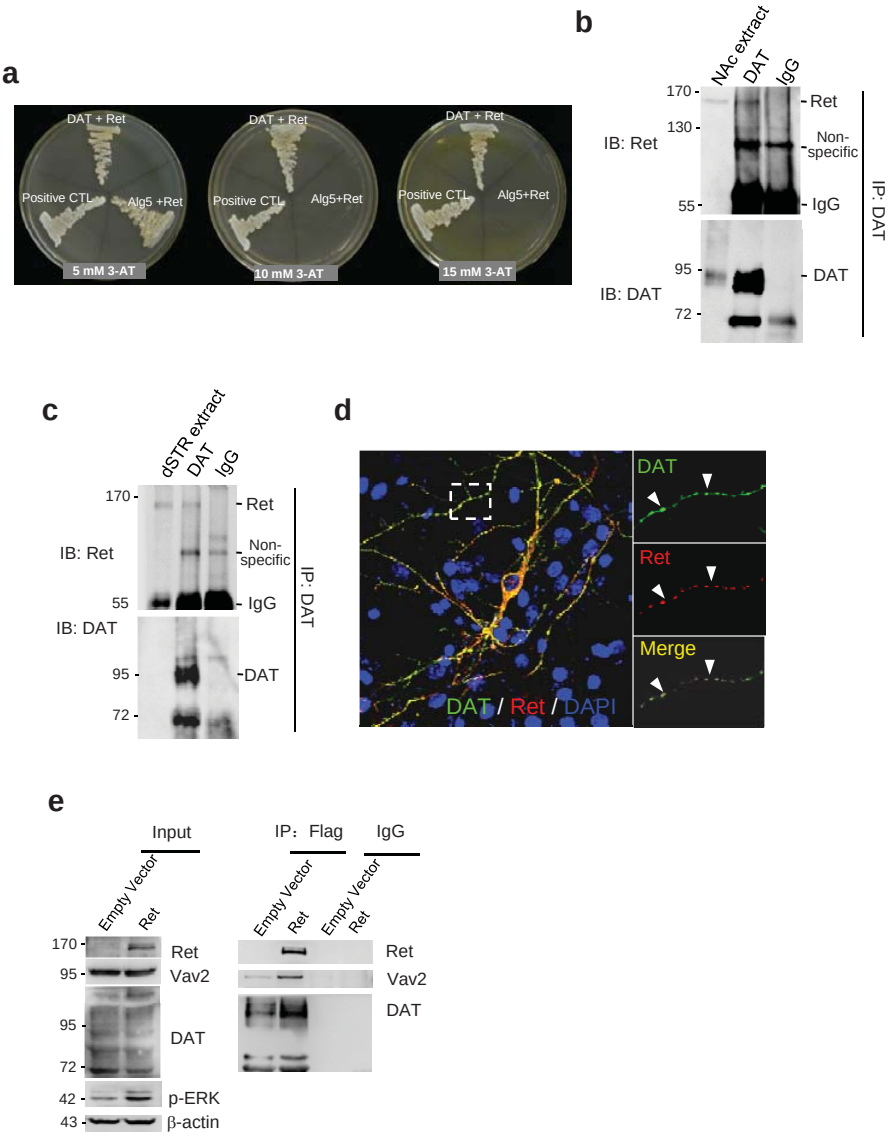
a
DAT + Ret
Positive CTL
Alg5 +Ret
5 mM 3-AT
DAT + Ret
Positive CTL
Alg5+Ret
10 mM 3-AT
DAT + Ret
Positive CTL
Alg5+Ret
15 mM 3-AT
b
NAc extract
DAT
IgG
170
130
55
IB: Ret
Ret
Non-specific
IgG
IP: DAT
95
72
IB: DAT
DAT
c
dSTR extract
DAT
IgG
170
IB: Ret
Ret
Non-specific
55
IgG
IP: DAT
IB: DAT
95
72
DAT
d
DAT
Ret
Merge
DAT / Ret / DAPI
e
Input
IP: Flag
IgG
Empty Vector
Ret
Empty Vector
Ret
Empty Vector
Ret
170
Ret
95
Vav2
95
DAT
72
42
p-ERK
43
β-actin
Ret
Vav2
DAT

Figure 6

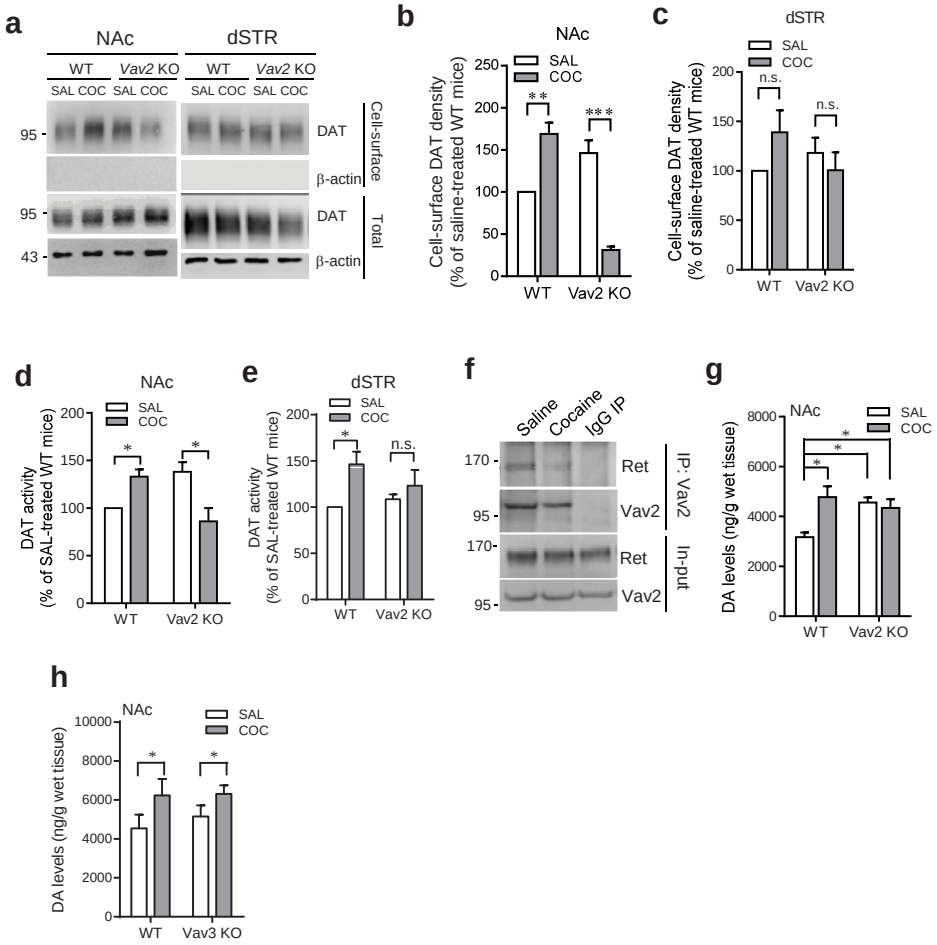
a
NAc
dSTR
WT
Vav2 KO
SAL COC SAL COC
SAL COC SAL COC
95
DAT
β-actin
Cell-surface
95
DAT
43
β-actin
Total
b
NAc
SAL
COC
Cell-surface DAT density
(% of saline-treated WT mice)
**
***
WT
Vav2 KO
c
dSTR
SAL
COC
n.s.
n.s.
Cell-surface DAT density
(% of saline-treated WT mice)
WT
Vav2 KO
d
NAc
SAL
COC
DAT activity
(% of SAL-treated WT mice)
WT
Vav2 KO
e
dSTR
SAL
COC
n.s.
DAT activity
(% of SAL-treated WT mice)
WT
Vav2 KO
f
Saline
Cocaine
IgG IP
170
95
Ret
Vav2
IP: Vav2
170
95
Ret
Vav2
In-put
g
NAc
SAL
COC
DA levels (ng/g wet tissue)
WT
Vav2 KO
h
NAc
SAL
COC
DA levels (ng/g wet tissue)
WT
Vav3 KO

Figure 7

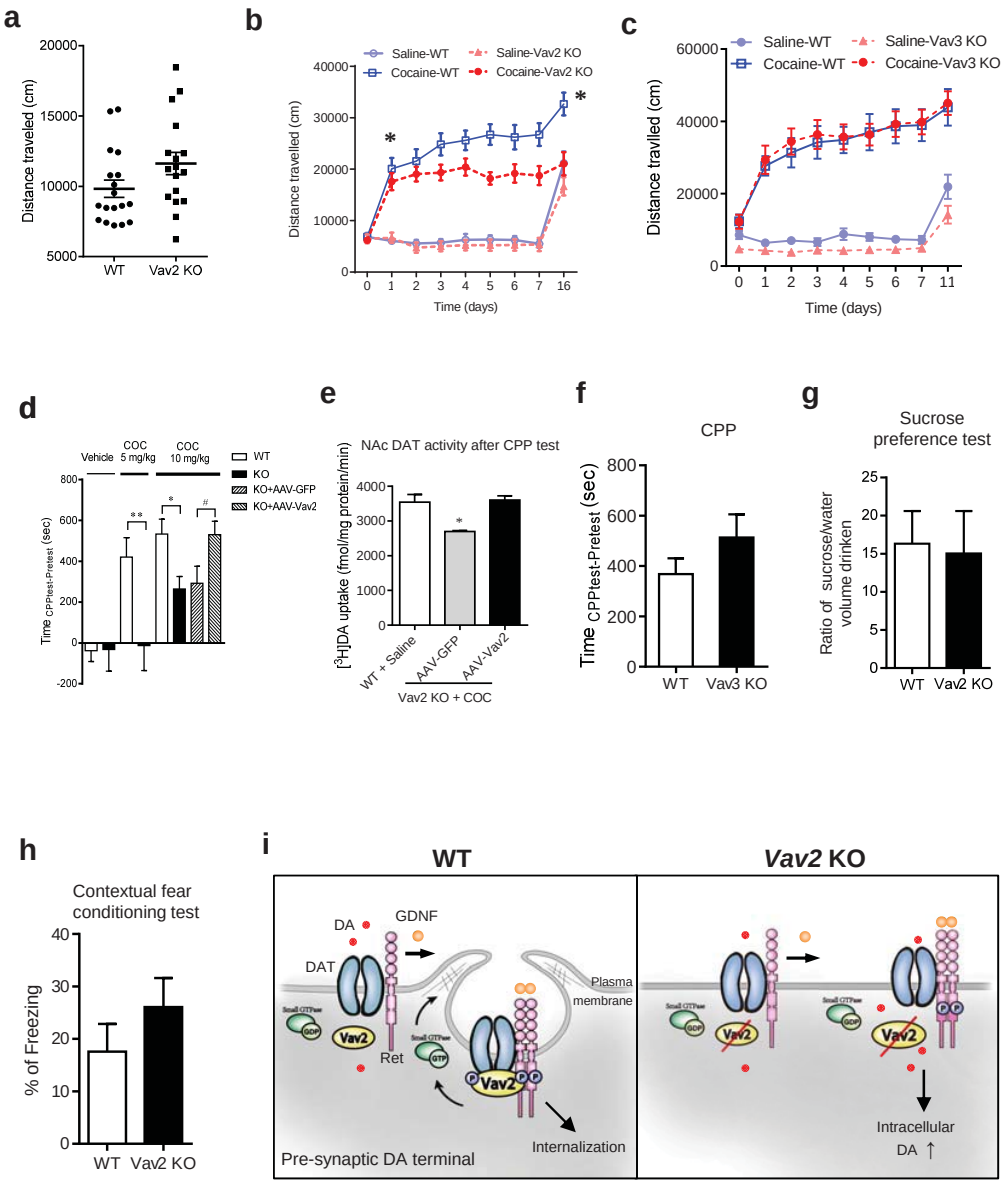
a
Distance traveled (cm)
WT
Vav2 KO
b
Saline-WT
Saline-Vav2 KO
Cocaine-WT
Cocaine-Vav2 KO
Distance travelled (cm)
Time (days)
c
Saline-WT
Saline-Vav3 KO
Cocaine-WT
Cocaine-Vav3 KO
Distance travlled (cm)
Time (days)
d
Vehicle
COC 5 mg/kg
COC 10 mg/kg
WT
KO
KO+AAV-GFP
KO+AAV-Vav2
Time CPPtest-Pretest (sec)
e
NAc DAT activity after CPP test
[3H]DA uptake (fmol/mg protein/min)
WT + Saline
AAV-GFP
AAV-Vav2
Vav2 KO + COC
f
CPP
Time CPPtest-Pretest (sec)
WT
Vav3 KO
g
Sucrose preference test
Ratio of sucrose/water volume drinken
WT
Vav2 KO
h
Contextual fear conditioning test
% of Freezing
WT
Vav2 KO
i
WT
Vav2 KO
DA
GDNF
DAT
Plasma membrane
Vav2
Ret
Internalization
Pre-synaptic DA terminal
Intracellular DA ↑

Supplementary Figure 1

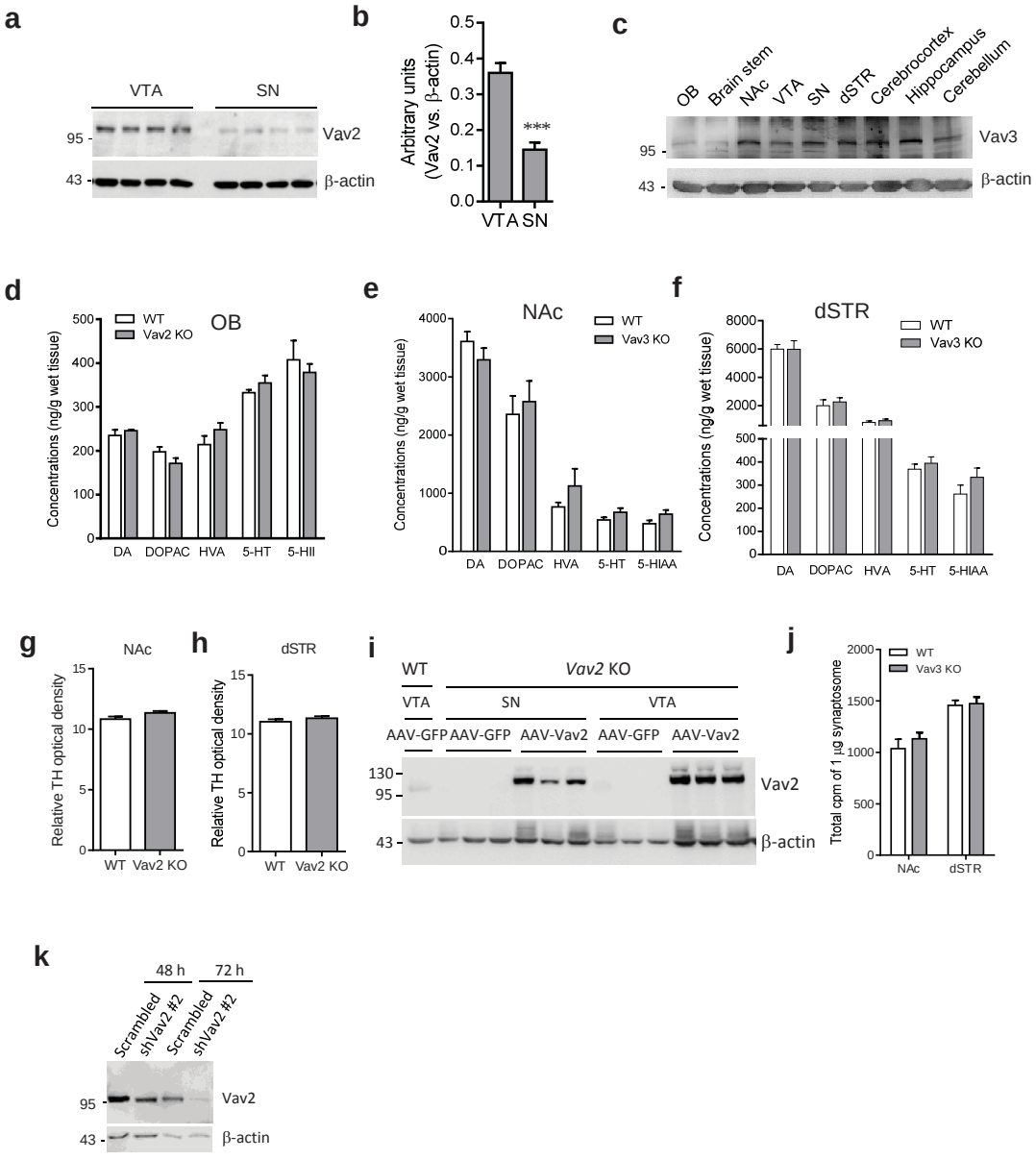

Supplementary Figure 1. Vav2, but not Vav3, is preferentially expressed in the VTA of adult mice, is required for the maintenance of dopamine homeostasis. (**a**) Immunoblotting reveals the Vav2 expression levels in the ventral tagmental area (VTA) is significantly higher than in the substantia nigra (SN) of adult brain. (**b**) Quantitative data of (**a**). Data are expressed as mean±S.E.M. (n=4); * $P<0.05$. (**c**) Western analysis of brain tissue lysates from adult mouse brain shows that Vav3 is ubiquitously expressed in major brain regions. The experiments were repeated at least twice. (**d**-**f**) Measurement of DA, 5-HT and their metabolites levels were performed in the olfactory bulb (OB) of *Vav2* KO mice (**d**, n=3), nucleus accumbens (NAc) (**e**, n=8~10) and dorsal striatum (dSTR) (**f**, n=8) of *Vav3* KO and wild-type mice. Data are expressed as mean±S.E.M.; * $P<0.05$. (**g**-**h**) Tyrosine hydroxylase immunosignal density was measured in the NAc (**g**) and dSTR (**h**) of *Vav2* KO and WT mice. Data are expressed as mean±S.E.M.; n=4 (**g**), n=4 (**h**), * $P<0.05$. (**i**) Western blotting shows that AAV-mediated overexpression of Vav2 following injection in the VTA or SN, validating the transfection efficiency in vivo. (**j**) [^{3}H]DA uptake assays were performed in the NAc or dSTR synapotosome preparation from *Vav3*-null and wild-type. Data are expressed as mean±S.E.M., n=3 per group. (**k**) Immunoblotting reveals that the levels of Vav2 expression were significantly down-regulated 48, 72 h following transfection with shVav2 #2 in N2a cells.

Supplementary Figure 2

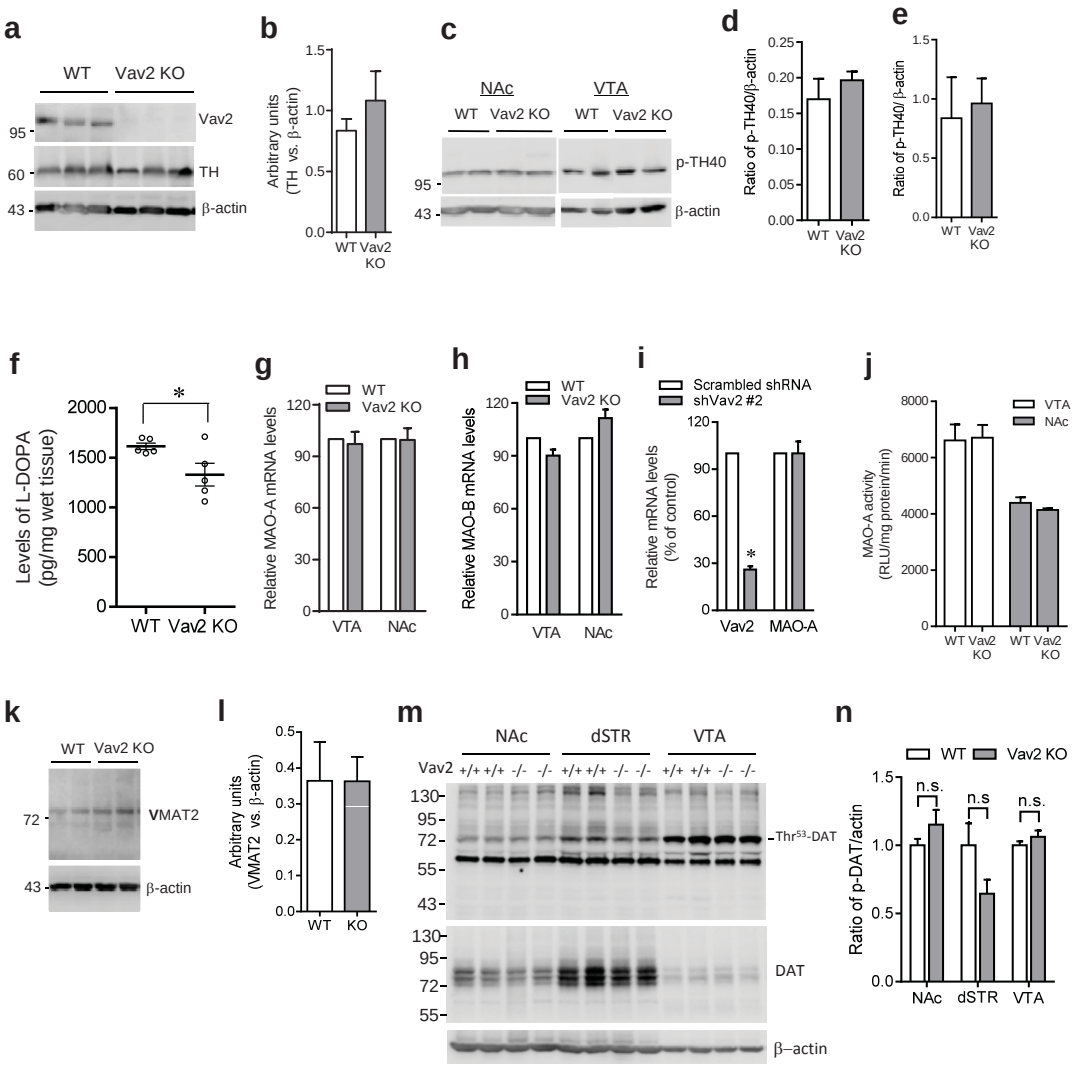

Supplementary Figure 2. DA biosynthesis and degradation in the NAc of *Vav2* KO mice are not significantly altered. (**a**) Western analysis of VTA tissue lysates from adult *Vav2*-null mouse brain in which rabbit monoclonal anti-Vav2 antibody was used, shows the absence of Vav2 protein. The experiments were repeated at least twice. (**b**) Quantitative data of (**a**). There is no significant difference in the levels of TH and VMAT2 protein expression between genotypes. Data are expressed as mean±S.E.M. (n=3 per group); **P*<0.05. (**c-e**) Western analysis of phospho-TH (ser 40) expression in the NAc (**c**, **d**) or VTA (**c, e**) of *Vav2* KO and WT mice. (**d**, **e**) Quantitative data of (**c**). Data are expressed as mean±S.E.M. (n=5-6). (**f**) The accumulation of L-dopa in the NAc was measured in the animals exposed to NSD-1015, an aromatic acid decarboxylase (AADC) inhibitor, using HPLC. Lower levels of L-dopa was seen in the NAc of *Vav2* KO mice, suggesting that TH enzymatic activity was markedly inhibited. Data are expressed as mean±S.E.M. (n=5 per group); **P*<0.05. (**g**-**h**) qPCR analysis of mRNA expression of MAO-A (**g**) and MAO-B (**h**), which are responsible for enzymatic degradation of 5-HT, NE and DA in the VTA and NAc of *Vav2* KO and WT mice. Data are expressed as mean±S.E.M. (n=3). (**i**) qPCR analysis of MAO-A and Vav2 mRNA expression in MN9D dopaminergic cell line transfected with shVav2 #2. Data are expressed as mean±S.E.M. (n=3). (**j**) Measurement of enzymatic activities of MAO-A were performed in the VTA and NAc of *Vav2* KO and WT mice. Data are expressed as mean±S.E.M. (n=3). (**k**) Immunoblotting reveals that the levels of VMAT2 expression were significantly altered in the striatum of Vav2 KO mice compared with wild-type counterparts. (**l**) Quantitative data shown in (**k**). Data are expressed as mean±S.E.M. (n=6). (**m**) Immunoblotting reveals that the levels of Thr53-DAT expression were not significantly changed between genotypes in various brain regions. (**n**) Quantitative data shown in (**l**). Data are expressed as mean±S.E.M. (n=5). n.s., not significant.

Supplementary Figure 3

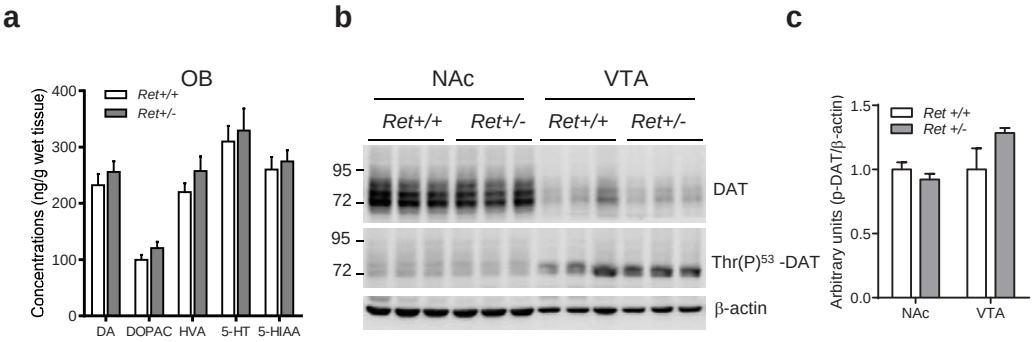

Supplementary Figure 3. (**a**) The levels of DA, 5-HT and their metabolites were measured in the olfactory bulb of *Ret+/-* and wild-type mice. The olfactory bulb (OB) is one of brain regions enriched in dopaminergic neurons. Data are expressed as mean±S.E.M. (n=5 per group). (**b**, **c**) Western blotting reveals that the levels of Thr^{53}-DAT expression are not significantly altered in the NAc and VTA between genotypes. (**c**) Quantitative data of (**b**). Data are expressed as mean ±S.E.M. (n=3 per group).

Supplementary Figure 4

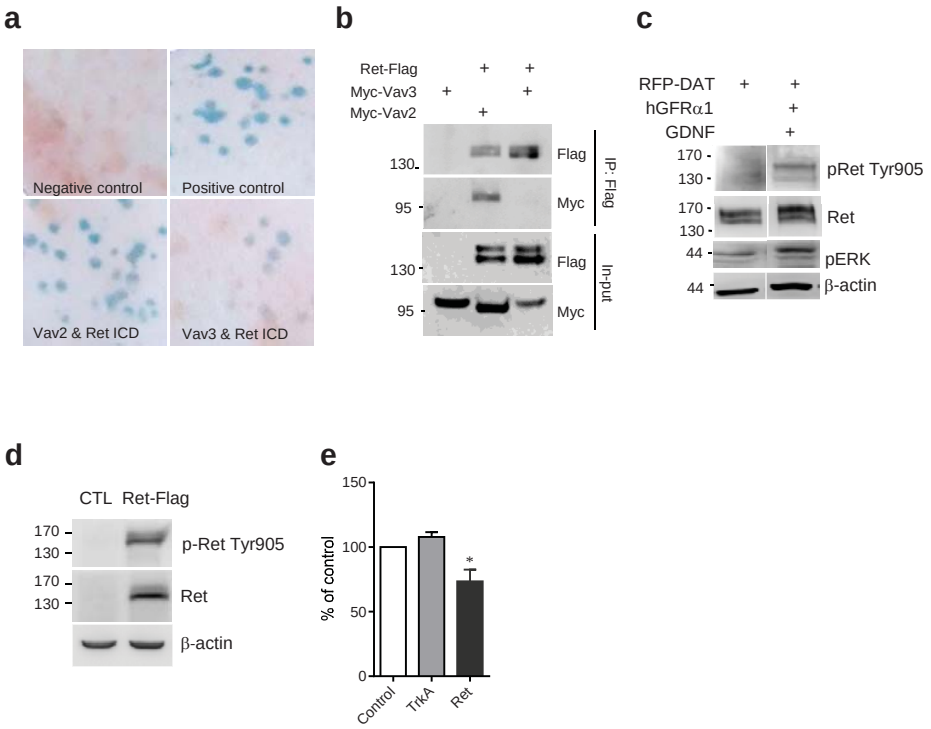

Supplementary Figure 4. Vav2, but not Vav3, strongly binds to Ret. (**a**) Y2H assays reveal that Vav2 strongly binds to Ret intracellular domain (ICD) . In contrast, Vav3 weakly interacts with Ret ICD. (**b**) Co-IP assays show that Ret-flag is immunoprecipitated with Myc-Vav2. (**c**) Western blotting reveals that treatment of N2a cells with 100 ng/ml GDNF increases the phosphorylation of Ret at Tyr905 site. (**d**) Western blotting reveals that overexpression of Flag-tagged Ret elevates the levels of phospho-Ret Tyr905 in 293T cells. These experiments were repeated at least three times. (**e**) [^{3}H]DA uptake assays reveal that overexpression of TrkA in HEK293 cells stably expressing YFP-DAT does not significantly alter DAT activity compared to control. Data are expressed as mean±S.E.M. (n=3).

Supplementary Figure 5

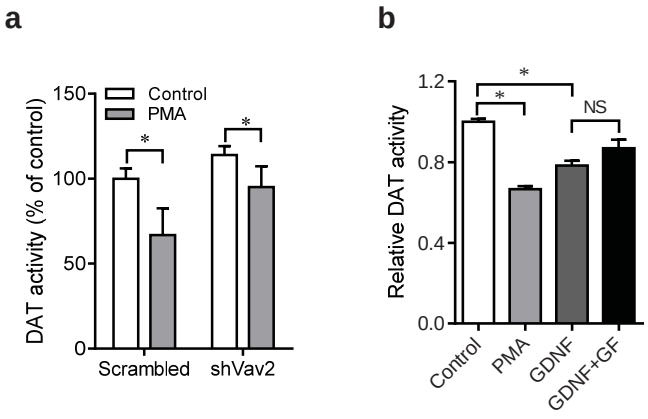

Supplementary Figure 5. Involvement of PKC in the Vav2-mediated DAT activity. (**a**) shVav2 #2-induced Vav2 knockdown attenuates PMA-induced reduction of DAT activity in N2a cells stably expressing RFP-DAT and GFRα1. Two-way ANOVA with Bonferroni's post-hoc test was performed. Data are expressed as mean±S.E.M. (n=3). **P*<0.05. (**b**) Treatment of N2a cells stably expressing RFP-DAT and GFRα1 with either PMA (1 μm, 30 min) or GDNF (100 ng/ml, 30 min) significantly down-regulate DAT-mediated DA uptake. These effects could not be significantly attenuated by pretreatment with PKC inhibitor GF-109203X (1 μm, 30 min). One way ANOVA with Bonferroni's post-hoc test was performed. Data are expressed as mean±S.E.M. (n=3). **P*<0.05.

Supplementary Figure 6

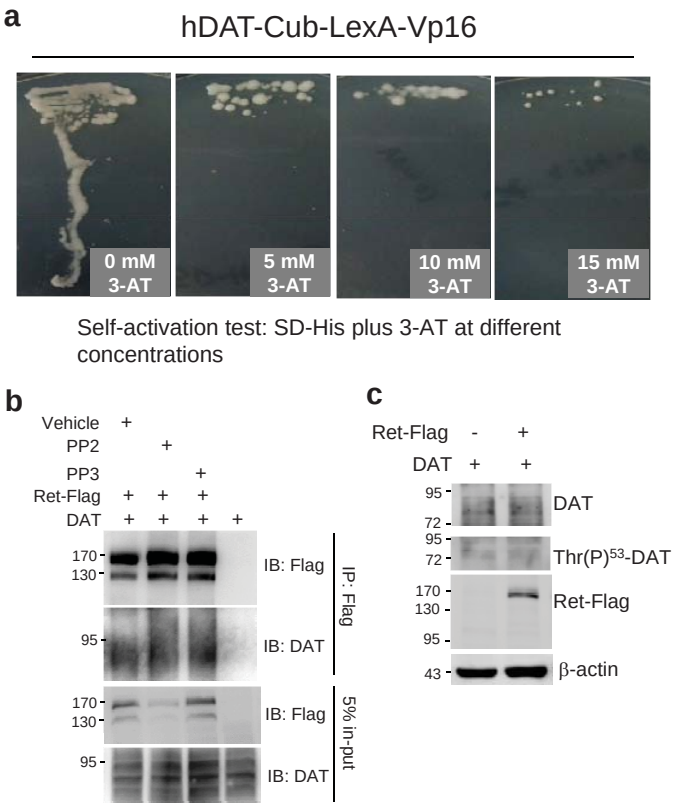

Supplementary Figure 6. Characterization of interaction among Vav2, DAT and Ret. (**a**) Colony growth assay on the SD-His medium showed the DAT-Cub-LexA-VP16 and Ret-NubG were expressed with no self-activation of the histidine reporter gene expression. (**b**) Co-IP assays show that treatment with PP2 does not alter their interaction between Ret and DAT in HEK293 cells. (**c**) Immunoblotting reveal that activation of Ret signaling by overexpression of Ret-Flag in HEK293 cells does not cause significant alteration in the levels of Thr(P)^{53}-DAT. These experiments were repeated at least twice.

Supplementary Figure 7

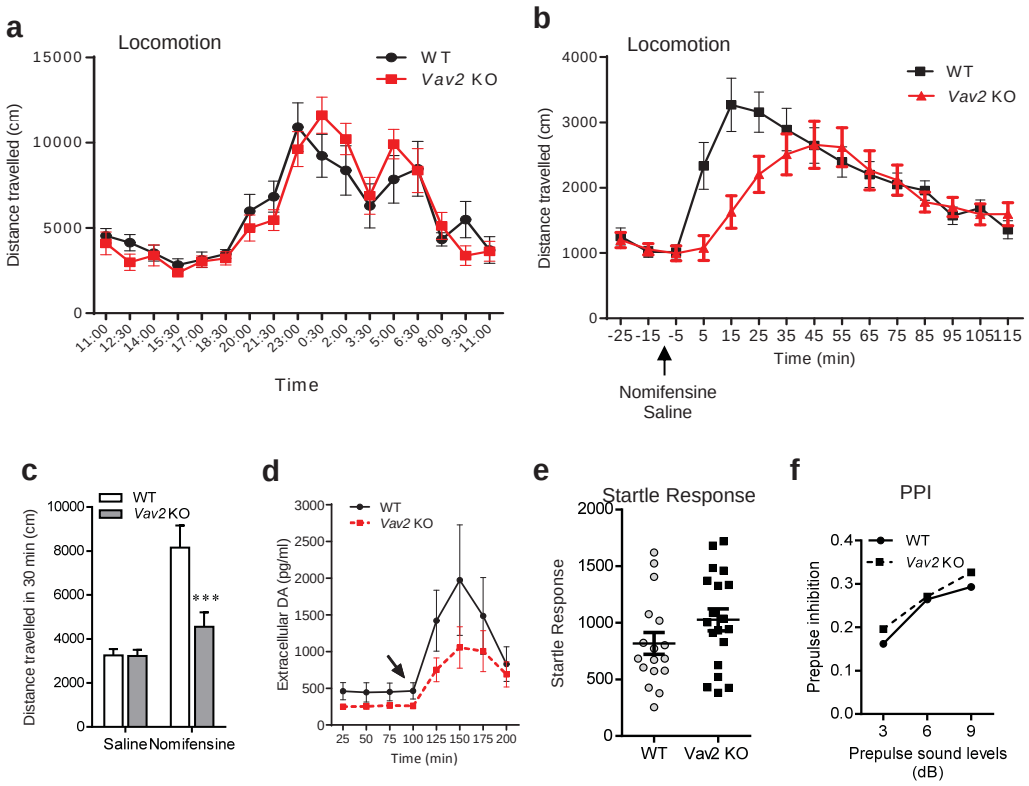

Supplementary Figure 7. Altered cocaine-induced behavioral response in *Vav2*-deficient mice. (**a**) The spontaneous activities are recorded during a 24-h period. There is no alteration between genotypes (n=5-7 per group). (**b**, **c**) The locomotor activity of *Vav2* KO administrated with nomifensine (10 mg/kg, i.p) is altered compared with WT mice (n=14 per group). (**d**) Measurement of extracellular DA concentrations in the NAc of WT and *Vav2* KO mice using *in vivo* microdialysis combined with HPLC analysis. The mice received single injection of cocaine (20 mg/kg, i.p.) as indicated by an arrow. Data are expressed as mean±S.E.M. (n=9-11). (**e**, **f**) The response to acoustic startle stimulation (**e**) and prepulse inhibition (**f**) is not significantly altered in *Vav2* KO mice compared with control (n=17-19/group).

Supplementary Figure 8

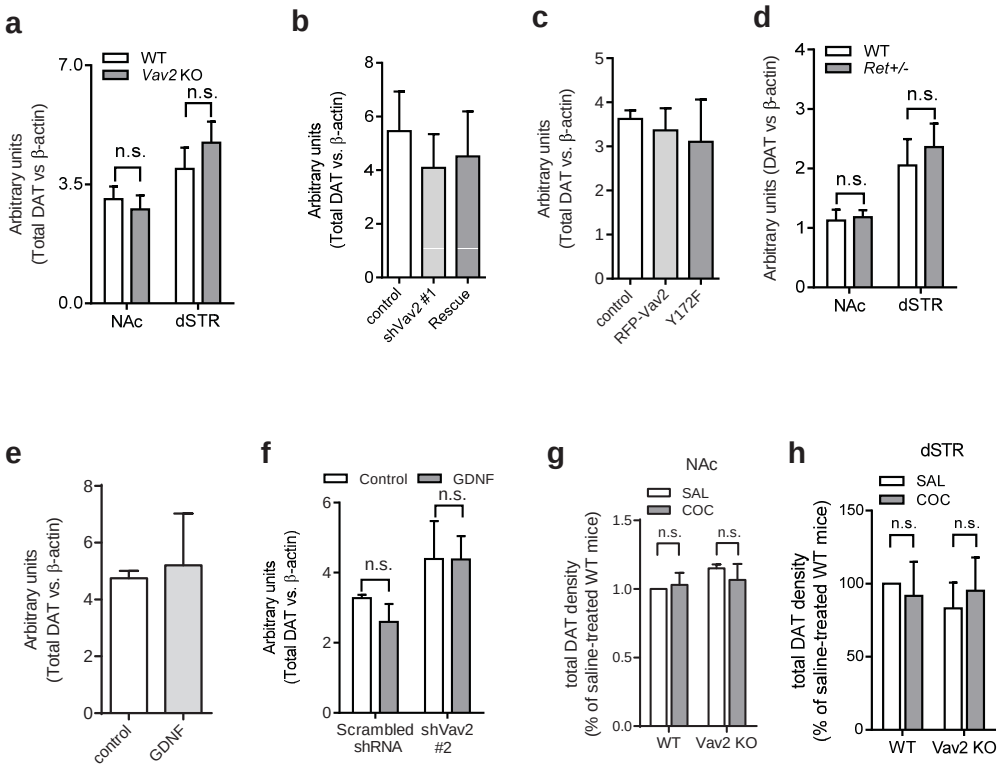

Supplementary Figure 8. Quantification of total DAT expression in the synaptosomal preparations derived from Vav2-null mice and wild-type control under various experimental conditions. The data are expressed as ratios of total DAT to β-actin. (**a**-**c**) correspond to Fig. 2f-i. (**d**) corresponds to Fig. 3b. (**e**, **f**) correspond to Fig. 4e, g. (**g**, **h**) correspond to Fig. 6b, c. n.s. no significance.

Shuyong Zhu et al.

SUPPLEMENTARY METHODS

Animals. Adult or neonatal C57BL/6 or C57BL/10 mice were from either Shanghai Laboratory Animal Center, Chinese Academy of Sciences or Jackson Laboratory, USA. *Vav2*$^{-/-}$ and *Vav3*$^{-/-}$ mice in a C57BL/10 (inbred) genetic background were used in the entire study. *Ret* heterozygous KO mice were purchased from the Jackson Laboratory (USA). GFP driven by TH promoter transgenic mice in a C57BL/6 genetic background were generous gifts from Dr. K Kobayashi (Riken BRC, Japan)[1]. Characterization and genotyping of these mice were described previously[2, 3, 4]. They were maintained on a 12 h light/dark cycle at 23°C with food and water available *ad libitum*. Five mice were housed in a cage. All procedures performed were approved by the Institutional Animal Care and Use Committee. Most of *in vivo* experiments were performed using male 8-12 week-old animals.

Plasmid constructions. A full-length human DAT (gift from Dr. XC Zhen) was subcloned into mammalian expression vectors pEYFP-C1 and pRFP-C1 (Clontech, Mountain View, CA, USA) or pEF-Flag (Shanghai Genomics, Shanghai, China)[5] to produce YFP/RFP- or Flag-tagged DAT constructs, respectively. pEF-Ret-flag construct was generated by amplification from human Ret in pcDNA3 (kind gift of Dr. C He). Vav2 and Vav3 constructs were from Dr. XR Bustelo. All the site-directed mutation of were generated using the QuikChange® site-directed mutagenesis kit (Agilent Technologies, Santa Clara, CA, USA)[6]. All constructs were verified by sequencing.

***In situ* hybridization.** Adult mouse brains were fixed overnight in 4% paraformaldehyde at

4°C. *In situ* hybridization (ISH) was performed on cryosections (12 μm thick) with digoxigenin-labeled single-stranded RNA probes as described previously[7]. To prepare the Vav2 hybridization probes, the primers were designed to specifically amplify mouse Vav2 nucleotides 2625-3468, corresponding to Vav2 amino acid residue 757 to partial 3'-UTR by PCR and the product was cloned into the pGEM-Teasy vector (Promega, Madison, WI, USA). Sequences of primers used were as follow: forward, 5'-CAAGTCTCGGGAGCGAAC-3'; reverse, 5'-TGTGCAAGCTCTGGCTCC-3'. Some sections were further processed for TH immunohistochemistry using 3,3-diaminobenzidine (DAB, Sigma-Aldrich, St. Louis, MO, USA) as substrate following Vav2 ISH.

Immunofluorescence, confocal microscopy and image analysis. Fixed cell cultures or cryostat sections of brain were incubated with one primary antibody followed by incubation with secondary antibody conjugated with either Alexa555, Alexa488, Cy5 or Alexa647. The same specimen were then incubated with another primary antibody, followed by incubation with the appropriate secondary antibody. They were imaged using either a cooled CCD (DP72, Olympus, Tokyo, Japan) on a microscope (BX51; Olympus) or a laser confocal microscope (Leica, Bensheim, Germany). Data were obtained and processed using Adobe Photoshop 7.0 software (Adobe Systems).

The following primary antibodies were used: (a) rabbit anti-TH polyclonal antibodies (pAb; 1:500; Chemicon, Temecula, CA, USA, #AB152); (b) rat anti-DAT mAb (1:200; Chemicon, #MAB369); (c) mouse anti-TH mAb (1:500; Chemicon, #MAB318); (d) goat anti-Ret pAb (1:1000, Neuromics, Edina, MN, USA, #GT15002); (e) mouse anti-Flag mAb (1:1000, Shanghai Genomics, Shanghai, China, #SG4110-16); (f) rabbit anti-Vav2 pAb (1:15,

Sigma-Aldrich, USA, #HPA003224).

Co-immunoprecipitation analysis. To analyze protein interactions in vitro, approximately 1 x 10^7 HEK293 cells (Cell Bank, Chinese Academy of Sciences) were harvested 24~36 h post-transfection and lysed in 1 ml of RIPA buffer [50 mM Tris-Cl (pH 7.5), 150 mM NaCl, 10% glycerol (w/v), 0.5% sodium deoxycholate, 0.1% SDS, 1% NP-40, 1 mM EDTA and protease inhibitors]. Resulting lysates were subjected to immunoprecipitation with antibodies directed against the epitope tag as described previously[8]. To detect the interaction between Flag-DAT and endogenous Vav2 in HEK293 cell, the Flag coupling agarose beads (Shanghai Genomics) were used to immunoprecipitate Flag-DAT. To detect the interactions *in vivo* between Vav2 and Ret, 18~22 mg VTA tissues were dissected from approximately 9 adult mice and collectively lysed in a 450 μl RIPA buffer for 1 h, followed the subsequent immunoprecipitation using Protein A/G beads (Santa Cruz Biotechnology, Santa Cruz, CA, USA) precoated with 10 μg sheep anti-Vav2 polyclonal antibody[9]. To investigate the interaction between DAT and Ret, 25 mg striatal tissue from adult mice were lysed in 700 μl lysis buffer [50 mM Tris-Cl (pH 7.5), 150 mM NaCl, 10% glycerol (w/v), 1% Brij97 (Sigma-Aldrich), 0.2% Triton X-100, and protease inhibitor cocktails (Roche)]. Tissue lysates were subjected to immmunoprecipitation with 7 μg rabbit anti-DAT polyclonal antibody (Millipore, Darmstadt, Germany, #AB1591P)[10]. Except for Vav2-DAT co-IP experiments in which the resulting beads were washed by RIPA lysis buffer with a high salt concentration of 300 mM NaCl, all the resulting immunoprecipitates were washed in lysis buffer 3 times for 45 min, and then subjected to immunoblot analysis with related primary antibodies. The

following primary antibodies were used: sheep anti-Vav2 pAb (1:200, Calbiochem, or Abcam, Cambridge, UK, #ab16135)[9], rabbit anti-DAT pAb (1:50, Millipore, #AB1591P), mouse anti-Flag mAb (1:100, Shanghai Genomics), mouse anti-Myc mAb (1:500, Santa Cruz Biotechnology).

Microdissection of GFP-labeled adult mouse tissue. Mice were sacrificed by decapitation and the brains were removed within 5 min postmortem. To obtain VTAs and SNc, mouse midbrain of transgenic mice expressing GFP under the control of TH promoter was dissected into three slices on a pre-cooled glass plate under a fluorescent microscope (SZX12, Olympus, Japan). GFP-labeled neurons in each brain slice were viewed using fluorescence illumination and optical filters for visualizing GFP under epi-illumination. The tissues containing GFP-labeled cells were carefully dissected out using ophthalmic tweezers and a bistoury. Isolated VTA and SNc tissues were quickly frozen in dry ice and stored at -80^0C until use.

Western blot analysis and quantification. Western blotting was performed as described previously[11]. For DAT immunoblotting, samples were heated at 37^0C for 1 h instead of boiling. The following primary antibodies were used: (a) rabbit anti-Vav2 mAb (clone EP1067Y, 1:20,000, Epitomics, Burlingame, CA, USA, #1993-1)[12]; (b) mouse anti-phosphotyrosine mAb (clone 4G10, 1:3,000, Upstate Biotechnology, Lake Placid, NY, USA, #05-1050X); (c) rabbit anti-Vav3 pAb (1:1,000; Upstate Biotechnology, Lake Placid, NY, USA, #07-464)[13]; (d) mouse anti-β-actin mAb (1:5,000; Sigma-Aldrich, #A5441); (e) rabbit anti-Ret mAb (1:10,000, OriGene Technologies, Rockville, MD, USA, #TA307815); (f) rabbit anti-phospho-ERK1/2 pAb (1:1000; Cell Signaling Technology, #9101); (g) mouse anti-Flag

mAb (1:2,000, Shanghai Genomics, #SG4110-16); (h) mouse anti-Myc mAb (1:2,000, Shanghai Genomics, #SG4110-18); (i) rat anti-DAT mAb (1: 1,000, Chemicon, #MAB369); (j) mouse anti-TH mAb (1:5000, Chemicon, #MAB318); (k) rabbit anti-phospho-TH (Ser40) (1:1000, Cell Signaling Technology, #2791); (l) mouse anti-phospho serine mAb (16B4, 1:2,000, Santa Cruz Biotechnology, #sc-81514); (m) Rabbit anti-pDAT Thr53 pAb (1:1000, Phosphosolutions, Aurora, CO, USA, #p435-53); (n) Rabbit anti-pRet tyrosine 905 pAb (1:1000, Cell Signaling Technology, #3221); (o) Rabbit anti-VMAT2 pAb (1:1000, Chemicon, #AB1767). The membrane was washed and incubated for 1 h at room temperature with the corresponding secondary antibodies: (a) HRP-conjugated goat anti-rabbit IgG (1:10,000; Jackson ImmunoResearch Laboratories, West Grove, PA, USA); (b) HRP-conjugated goat anti-mouse IgG (1:10,000; Jackson ImmunoResearch Laboratories); (c) HRP-conjugated goat anti-Rat IgG (1:10,000; Jackson ImmunoResearch Laboratories); (d) HRP-conjugated goat anti-mouse IgM (1:10,000; Jackson ImmunoResearch Laboratories). Peroxidase activity was detected with SuperSignal WestPico chemiluminescent substrate (Pierce Biotechnology) and visualized and digitized with ImageQuant (LAS-4000, Fujifilm, Japan). Optical densities of bands were analyzed by using ImageReader software (Fujifilm) or ImageJ software (NIH). Protein levels, quantified by computer analysis as the ratio between each immunoreactive band and the levels of β-actin, were expressed as a percentage of vehicle-treated control.

Yeast two-hybrid assays. Ret intracellular domain (ICD) interacting proteins were identified by using yeast two-hybrid screening, as described previously[14]. Briefly, the Ret ICD and Vav2 cDNAs were subcloned into the yeast expression vector pGBT7 and pACT2,

respectively (Clontech). Yeast strain Y190 cells were transformed using the lithium acetate method. Positive clones were identified by colony selection on plates lacking leucine, tryptophan, and histidine (-Leu-Trp-His) supplemented with 30 mM 3-amino-1,2,4-triazole (3-AT). Their interactions were verified using a β-galactosidase assay.

To investigate the interaction between Ret and DAT, the yeast split-ubiquitin membrane protein two-hybrid assay was performed as described previously[15]. Previous studies demonstrated that both the full-length Ret and DAT can be used as functional baits for the split-ubiquitin based yeast two hybrid screening[16, 17], indicating Ret and DAT with all their transmembrane domains were expressed with correct orientations and membrane locations. Human DAT and Ret cDNAs were subcloned into the vector pCCW-STE and pDSL2xN (Dualsystems Biotech AG, Schlieren, Switzerland), respectively. Upon mix-transform into the yeast strain NMY32 (Dualsystems Biotech), the fusion proteins of DAT-CUB-LexA-VP16 and Ret-NubG could be produced. The physical binding of DAT and Ret was identified by colony selection in selective medium lacking leucine, tryptophan, and histidine (-Leu-Trp-His) supplemented with varying levels of 3-AT. To test the self-activation on histidine reporter gene expression, the yeast NMY32 cells transformed with pCCW-STE-DAT were re-grown onto the selective medium lacking leucine, and histidine (-Leu-His) supplemented with increasing concentrations of 3-AT.

Glutathione S-transferase (GST) pull-down. The human Vav2 C-terminal fragment containing SH3-SH2-SH3 domain was amplified by PCR, and the product was subcloned into the bacterial expression vector pGEX-6P-1. Recombinant fusion protein of GST-Vav2

C-terminal fragment was expressed in the bacterial strain BL21 (Novagen) and purified with glutathione sepharose 4B according to the instructions of the manufacturer. The protein purification was monitored at each step by SDS-PAGE followed by Coomassie staining. For pull downs, human Ret-Flag or Ret Y905F-Flag were transiently overexpressed in the HEK293 cells, which were lysed in RIPA lysis buffer [50 mM Tris-Cl (pH 7.5), 150 mM NaCl, 10% glycerol (w/v), 0.1% SDS, 1% Triton X-100, 1% NP-40, 1 mM EDTA and protease inhibitors]. The whole cell lystes were incubated with the GST-Vav2-C fusion proteins overnight, which could be trapped by slurry of glutathione-agarose beads. After incubation, beads were washed three times with RIPA lysis buffer and suspended into 60 μl loading buffer. The supernatant were subjected to Western blotting using primary antibodies against Flag or GST.

Crude synaptosomal preparations. Crude synaptosomes were prepared as described previously[18]. Briefly, the NAc and dSTR were dissected from adult mouse brain and homogenized with the Teflon pestle manually for 100 up-and-down strokes on ice in at least 10 volume of 0.32 M sucrose. The homogenates were centrifuged at 1,000 g for 10 min at 4°C. The supernatants were carefully collected and transferred into new centrifuge tubes, which were subjected to second centrifugations at 12,800 g for 20 min at 4°C. The pellets were the crude synaptosomes, which were either diluted in PBS plus 0.1 mM Ca^{2+}, 1 mM Mg^{2+} for protein biotinylation, or diluted in dopamine reuptake buffer for analyzing DAT transporter activity, after the protein concentrations were measured using the Bradford protein assay. The NAc or dSTR were pooled from at least four mice based on the experiments conducted, and in such a way, all the experiments were repeated at least three times.

Membrane protein biotinylation. Biotinylation reactions were performed using a Cell

Surface Protein Isolation Kit (Pierce, Rockford, IL, USA, #89881). Briefly, about 1×10^6 cultured HEK293 or N2a cells were washed with ice-cold PBS plus 0.1 mM Ca^{2+} and 1 mM Mg^{2+} for three times. The EZ-Link sulfo-NHS-SS-biotin reagent (Pierce, dissolved in 1 mg/ml in PBS with 0.1 mM Ca^{2+} and 1 mM Mg^{2+}) was added onto the cell dish for 1 h at 4°C, with occasional stirring. The reaction was terminated by incubation in the presence of quenching buffer (Pierce), followed by washing with the termination buffer (Pierce) for three times. After termination, 450 µl lysis buffer (Pierce) was added and incubated for 1 h on ice. The cell lysates were further incubated with 150 µl slurry of streptavidin resins (Pierce) for overnight at 4°C. The resins were collected by centrifuging at 1,000 g for 5 min at 4°C and washed with 1 ml washing buffer (Pierce) for twice. After the last centrifugation, the precipitates of resins were diluted in 60 µl loading buffer containing 3% SDS and 100 mM DTT for 1 h at 37 °C. The supernatant were subjected to Western blotting. For biotinylation of fresh-prepared crude synaptosomes, approximately 800-1,000 µg proteins of crude synaptosomes were diluted in PBS and labeled with 1 mg/ml EZ-Link Sulfo-NHS-SS-Biotin reagent for 1 h at 4°C. After quenching the reaction, the synaptosome were collected by centrifugation (12,800 g, 20 min, 4 °C) and diluted in 500 µl RIPA lysis buffer [50 mM Tris-Cl (pH 7.5), 150 mM NaCl, 10% glycerol (W/V), 0.1% SDS, 1% Triton X-100, 1% NP-40, 1 mM EDTA and protease inhibitors]. The biotin-labeling synaptosome were lysated using sonication (150 W power, 5 seconds, 1 time) within RIPA lysis buffer. After additional centrifugation (12,800 g, 20 min, 4°C), the supernatant were incubated with 150 µl slurry of streptavidin resins (Pierce) for overnight at 4°C. The resins were collected, washed and conjugated proteins were eluted as described above. All protein samples including the in-puts were incubated at 37 °C for 1 h before SDS-PAGE.

[^{3}H]DA uptake assays. DAT transporter activity measurements were carried out as described previously[5, 19, 20]. Briefly, aliquots (30-50 μg proteins) of synaptosomal preparations were incubated at 25°C for 10 min in a total volume of 0.5 ml of uptake buffer [5 mM Tris, 7.5 mM HEPES, 120 mM NaCl, 5.4 mM KCl,1.2 mM $CaCl_2$, 1.2 mM $MgSO_4$, 100 nM desipramine (Tocris Bioscience), a norepinephrine transporter blocker, 1 μM pargyline, 2 mg/ml glucose (pH 7.1)] in the presence of 20 nM [^{3}H]DA (dihydroxyphenylethylamine 3,4-[ring-2,5,6,-^{3}H], PerkinElmer). Non-specific [^{3}H]DA uptake was defined in the presence of 10 μM GBR 12909 (Tocris Bioscience), a specific DAT inhibitor. After the incubations, the assays were terminated by placing the tubes on ice for 10 min. The synaptosomal solutions were then transferred onto glass fiber C Whatman filters (Sigma-Aldrich) pre-coated with 0.3% polyethylenimine to remove residual unbound [^{3}H]DA. The filters were washed three times with 2 ml ice-cold saline, air dried, and put into scintillation vials. Up to 4 ml scintillation cocktails were added for counting using a liquid scintillation counter (Beckman LS6500). Specific DA uptake was obtained by subtracting the non-specific uptake from the total radioactivity. For the kinetic assay, 30-50 μg fresh synaptosomes were used to incubate with 2.5 ~180 nM [^{3}H]DA at 25°C for 10 min in a total volume of 0.5 ml of uptake buffer. Non-specific [^{3}H]DA uptake was defined as uptake in the presence of 10 μM GBR 12909. Kinetic parameters were determined by nonlinear regression fitting using Prism software (GraphPad Prism). V_{max} and K_m values for DA uptake were obtained using the generalized Michaelis-Menten equation (GraphPad Prism).

For the DA uptake assay in cultured HEK293 cells, cells were seeded onto 24-well plates, and [^{3}H]DA uptake was measured 72 h after shRNA transfection. Culture media were

removed following washing with 1 ml uptake buffer. [^{3}H]DA uptake was initiated by adding 500 µl uptake buffer per well containing 20 nM [^{3}H]DA. Assays proceeded for 10 min at 37°C and were terminated by rapidly rinsing cells with ice-cold uptake buffer for three times. Cells were solubilized in 0.5 ml of 1% SDS and agitated for 1 h. Accumulated radioactivity was determined by a scintillation counting. To assay DA uptake activities in primary ventral mesencephalic neurons, the cells were maintained in 24 well plate and incubated in a total volume of 500 µl uptake buffer with 100 nM desipramine per well containing 20 nM [^{3}H]DA at 37°C for 10 min. To assay DA uptake activities in N2a cells stably expressing both human GFRα1 and RFP-DAT, cells were incubated in a total volume of 500 µl uptake buffer with 100 nM desipramine per well containing 20 nM [^{3}H]DA at 37°C for 10 min, followed by serum-starvation of 7 h in DMEM and the subsequent 30 minutes' stimulation of GDNF (100 ng/ml, PeproTech, London, UK). Measurements of radioactivity were performed as described above. Non-specific [^{3}H]DA uptake was defined in the presence of 10 µM GBR 12909.

Mesencephalic neuronal culture. Primary VM neuronal cultures were prepared as described previously[21]. Briefly, fetuses obtained from pregnant mice on the 16th gestational day (E16, where E0 is the day of the vaginal plug) were used for preparation of VTA neuronal cultures. The animals were sacrificed with overdose of pentobarbital sodium and the brain region corresponding to the VTA tissues were collected and digested with papain. Cell suspension was plated onto poly-L-lysine coated 24-well plates at a density of 10^5 cells/cm^2 in DMEM/Ham's F12 medium (Invitrogen, Carlsbad, CA, USA) containing 10% fetal bovine serum (Invitrogen). Cells were maintained at 37°C in a 95% air-5% CO_2 humidified atmosphere for 3 h, and the cells were then switched to Neurobasal medium with 2% B27 supplement (Invitrogen) and were maintained for at least 7 days. GDNF was added on the last

day and incubated for 30 minutes before the cultures analyzed for DAT-mediated DA uptake or DAT internalization.

Cell culture and transfections. HEK293 cells and N2a cells were maintained at 37°C, 5% CO_2 in DMEM/Ham's F12 medium (Invitrogen) containing 10% fetal bovine serum (FBS, Invitrogen) supplemented with 2 mm glutamine and penicillin/streptomycin. HEK293 cells stably expressing human YFP-DAT, or N2a cells stably expressing both human GFRα1 and RFP-DAT were maintained under selective pressure with 200 μg/ml G418 (Invitrogen). The HEK293 cells were transiently transfected with indicated vectors using a standard calcium phosphate protocol, while N2a cells were transfected using the Lipofectimine 2000 (Invitrogen).

Cannulation surgery. The mice were anaesthetized with pentobarbital sodium (70 mg/kg i.p.) and attached from outer ear canals to the stereotaxic device (RWD Life Science Co., Ltd, Shenzhen, China). The coordinates for guide cannula (CMA/7; CMA/Microdialysis, Stockholm, Sweden) were calculated relative to bregma and guide cannulas were aimed at the point above the nucleus accumbens (A/P, +1.5 mm; L/M, +0.9 mm; D/V, 4.0 mm) according to a stereotaxic atlas[22]. Cannulae were attached to the skull with dental cement and fastened one stainless steel screw. After the surgery, mice were placed into individual test cages and allowed to recover in the cages for at least three days before the experiment.

***In vivo* microdialysis.** In vivo microdialysis was performed as described previously[23]. Briefly, at approximately 10 AM on the experiment day, a microdialysis probe (CMA/7, 1.0-mm membrane, o.d. 0.24 mm) was inserted into the guide cannula, and the probe was infused with

a modified Ringer solution (147 mM NaCl, 1.2 mM $CaCl_2$, 2.7 mM KCl, 1.0 mM $MgCl_2$ and 0.04 mM ascorbic acid) at a flow rate of 1 μl/min for 1 h. The collection of actual microdialysis samples (every 25 min, 25 μl/sample) was then started. In some experiments, the mice were pretreated either with or without cocaine HCl (20 mg⁄kg, i.p.) daily for three consecutive days. On the experiment day, all mice received 20 mg⁄kg cocaine (i.p.) and the samples were collected for 2 h after the injection. The effects of cocaine on the dopamine output were presented as relative to the baseline (the average concentration of four consecutive stable samples defined as 100%). The positions of the probes in the brains were verified histologically at the end of experiment.

Monoamine measurement using HPLC. The concentrations of dopamine, noradrenaline, 3,4-dihydroxyphenylacetic acid (DOPAC), homovanillic acid (HVA), serotonin (5-HT) and 5-hydroxyindoleacetic acid (5-HIAA) in microdialysis perfusates were determined by HPLC with an electrochemical detector (Coulochem III, ESA, USA) equipped with a model 5041 Analytical cell, a ESA 584 HPLC pump (ESA Biosciences Inc. USA). The mobile phase (100 mM NaH_2PO_4, 50 mM citric acid buffer, 200 mg/l sodium 1-octanesulfonate, 7-10% methanol and 50 μM EDTA, pH 3.0) was delivered at a flow rate of 0.2 ml/min to a reverse phase Eclipse Plus C18 column (4.6 × 30 mm, 3.5-μm threaded, Agilent Technologies). Twenty-two microlitres of the dialysate sample was injected onto the HPLC system. Peak identification and quantification were conducted using the EZ Chrom SI ChemisSation software (version 3.2, Agilent Technologies).

To measure monoamine content of mice brain, animals were killed by decapitation, and the NAc and dSTR were rapidly dissected out. Tissue was homogenized in 0.4 M perchloric acid (30-50 μl/mg tissue) on ice and centrifuged at 16,000 rpm for 30 min. Supernatants were

collected and diluted at 1:5 for analysis. Up to 100 µl of each sample were injected into the HPLC system. To measure accumulated L-dopa, mice were administrated with 100 mg/kg NSD-1015 (Sigma-Aldrich, i.p.), and NAc tissue punches were taken 30 minutes later and processed as described above.

Vav2 knockdown. shRNA targeting human, rat and mouse Vav2 (designed as ShVav2 #1) was a gift from Dr. DD Billadeau[24]. The sequences were as follows: shVav2 #1, 5'-GGACATTGAGAAGAACTAC-3'; scrambled shRNA, 5′-GACGAAGCCGAAAGTTTAA-3'. shRNA Vav2 specifically target mouse Vav2 was also designed and was designated as shVav2 #2. The sequences were as follows: shVav2 #1, 5'-GACAAATTTGGACTAAGAA-3', scrambled shRNA, 5'-GCAATTAGTGAATAGACAA-3'. They were cloned into pSicoR vector to generate pSicoR-shVav2 and pSicoR-scrambled as previously described[25].

Constructs and *in vitro* packaging of AAV-Vav2. The mouse Vav2 cDNA was sublconed from pA1-flag-Vav2 constructs (obtained from XR. Bustelo). The Flag-tagged Vav2 expression is driven by the human synapsin 1 (hSyn) gene promoter in these virus particles. The sequence of 2A signal peptide was derived from plenti-2A-EGFP plasmid. AAV2 backbone was cloned from pAAV-hSyn-eNpAC-WPRE plasmid (gift from ZL Qiu). For AAV-hSyn-mVav2-2A-EGFP plasmid, 2A-EGFP was first inserted into AAV backbone with Age1 and EcoR1 followed by insertion of mVav2 into the AAV-hSyn-2A-EGFP with fast seamless cloning kit (DoGene Inc.). The AAV2 helper vectors, pXX680 and pXX2 were originally purchased from University of North Carolina at Chapel Hill. The AAV2 viruses were generated as previously described[26]. In brief, HEK293TN cells were transfected with

two helper vectors, pXX680 and pXX2 and one AAV vector. Seventy-two hours after transfection, the viruses were purified from the cell lysates by using a heparin-agarose column and concentrated to the final volume. The control virus AAV- hSyn-GFP was purchased from the NeuronBiotech (Shanghai, China) with titer 1.65 x 10^{13} infections units per ml. The AAV-hSyn-mVav2-2A-EGFP virus titer was measured with qPCR. The primers were as follows: GFP: Forward, 5'-CAACAGCCACAACGTCTATATCATG-3'; Reverse, 5'-ATGTTGTGGCGGATCTTGAAG-3' [27].

AAV-Vav2 stereotactic injection. For viral injection in the brain *in vivo*, mice were anesthetized with pelltobarbitalum natricum (70 mg/kg of body weight, i.p.) and placed in a stereotactic frame. Mice were injected bilaterally with 2 μl of purified and concentrated AAV virus (~10^{13} infections units per ml) into the VTA (coordinates from the bregma: −3.4 mm anterior/posterior, ±1.3 mm medial/lateral, −4.1 mm dorsal/ventral, with 14° angle toward the midline in the coronal plane) or SNc (coordinates from the bregma: −3.1 mm anterior/posterior, ±1.3 mm medial/lateral, −4.4 mm dorsal/ventral) using glass microelectrodes at a rate of 100 nl/min. The injection microelectrode was slowly withdrawn 5 min after the virus infusion. The animals received AAV virus sterotactic injection in brain were maintained for 1 or 5 weeks post-surgery, respectively.

Monoamine oxidase-A (MAO-A) enzymatic activity assay. MAO-A enzyme activities were measured in VTA and NAc protein extracts with the luminescent MAO-Glo assay kit (Promega) according to the manufacturer's instructions. In brief, the brain regions corresponding to the VTA and NAc were pooled from adult mouse brains, and lysed by sonication in 100 mM HEPES plus 5% glycerol and protease inhibitor cocktail, pH 7.5. Total MAO-A activity was assayed by incubation of 1 or 5 μg VTA or NAc protein (quantified by

Bradford assay) in a total volume of 50 μl containing MAO-A substrate modified by luciferin and enzyme reaction buffer at 37°C for 20 min. After incubation, the luminescence intensities of luciferin were assayed using a luminescence reader[28]. Total MAO-A activity was plotted as RLU/mg protein/min.

RNA isolation and quantitative PCR. Isolation of total RNA was performed as described previously[7]. Briefly, brain tissue of young male mice were homogenized in TRIzol reagent (Invitrogen). cDNA was synthesized from 1 μg of extracted total RNA using M-MLV Reverse Transcriptase kit (Invitrogen) according to the manufacturer's protocol. Quantitative PCR was performed with SYBR-Green premix Ex Taq (Takara, Japan) and detected by a Real Time PCR System (Roche LightCycler 480 or Rotorgene 6000). β-actin was used as an internal control gene. qPCR primers were designed using Primer Picking Program and their sequences were as follows: Vav2, forward, 5'- TGGACTAAGAAACAGTGAGC-3', reverse, 5'-TGTCTCCTCTGATGGAAATG-3'; MAO-A, forward, 5'-AGTAGGCAGGATTTACTTTGCAG-3', reverse, 5'-GCAACTTTTCCTAGAGCATTC-3'; MAO-B: forward, 5'- GAAGTTGAGCGGCTGATACAC -3', reverse, 5'-GCATCACTGGGAATCTCTTGG-3'; β-actin, forward, 5'-GAGATTACTGCCCTGGCTCCTA-3', reverse, 5'-TCATCGTACTCCTGCTTGCTGAT-3'. Following PCR amplification, a first derivative melting-curve analysis was performed to confirm the specificity of the PCR. The relative fold difference in mRNA between samples was calculated by comparing the threshold cycle (C_t) at which product initially appeared above background according to: $2^{-(\Delta Ct)}$, where ΔC_t is the difference between control group and a treatment group.

Quantitative analysis of TH-positive fibers. The optical density of TH immunoreactive

terminals or processes of the NAc and dSTR of adult Vav2 KO and wild-type mice was assessed using a method described previously with a few modifications[29]. Briefly, image capture of the whole tissue slide was performed in four coronal sections corresponding to plates 19, 22, 25, and 34 in the mouse brain atlas[22] using Neurolucida microscope imaging system (E600FN, Nikon, Japan). TH fluorescent signals were accessed by ImageJ software in sections through the NAc (plates 19, 22, 25) and dSTR (plates 19, 25, 34). The TH-negative area (the cortex) of each section served as the background and the mean gray value of the total TH+ area which was subtracted by the background represent the density of TH+ terminals.

Behavior assays

Most of behavioral tests usually began in the morning approximately at 10 am.

Spontaneous motor activity and motor response induced by drugs. Spontaneous locomotor activity in a 30 min period was measured in an activity cage (45 x 45 cm) and analyzed by using a video tracking software package (EthoVision XT, Nodlus, Netherlands). Cumulative horizontal motor activity was recorded for 30 min.

Eight-twelve-week-old mice were administrated with cocaine (20 mg/kg, i.p.) or saline once a day for eight consecutive days. After each injection, mice were placed in 25×25 cm clear plastic cages equipped with AniLab Systems (China) for 1 h. On challenge day, mice were injected with cocaine (20 mg/kg) and placed back in the cage for 1 h. Locomotion was assessed as distance traveled for 1 h following each injection.

To evaluate motor effects induced by nomifensine, a DAT inhibitor, animals of each genotype were injected with 0.9% NaCl (0.01 ml/g body weight, i.p.) and placed into the activity boxes

for 30 min period of habituation. After the habituation period, the mice were injected with nomifensine (10 mg/kg, i.p.) and placed into the same activity boxes for a 2 h recording period.

Conditioned place preference (CPP). CPP was tested in a rectangular Plexiglass shuttle box as described elsewhere[30] with a few modifications. Briefly, the apparatus consisted of three compartments, one with black walls and the other with white walls separated by a guillotine door. In the pre-test (Phase I), mice were allowed to explore the two compartments of the shuttle box for 15 min each day with the guillotine doors opened for 3 consecutive days. During the conditioning period (Phase II lasting 8 days between day 2 and 9) mice received four i.p. injections of saline and four of cocaine (5 or 10 mg/kg) at 24 h intervals. On odd training days (i.e. 1, 3, 5 and 7), each mouse received saline i.p. and was immediately placed in the unpaired (black) compartment for 30 min. On even days (i.e. 2, 4, 6 and 8) each mouse was injected i.p. with cocaine and was immediately placed in the cocaine-paired compartment, the white one, for 30 min. Control mice received saline only. On the test day (Phase III, day 10), mice were individually placed at the intersection of the two compartments with free access to both sides. Neither cocaine nor vehicle was administrated. The time spent in each compartment was recorded over 30 min. The increase in the time spent in the white compartment indicates reinforcing properties.

Contextual fear conditioning test. Contextual fear conditioning test was carried out as described previously[31] with minor modifications. Briefly, mice were placed in a fear conditioning chamber (Med Associates, USA) and allowed to acclimate for 5 min. After the initial acclimation, mice received three foot shocks at 120, 152 and 184 sec, respectively using lower shock intensity of 0.5 mA (constant current, 2 sec). Mice were then placed back

to their home cages 2 min after the final foot shock. Freezing behavior was measured as the amount of time exhibiting freezing behavior during each intershock interval. To study contextual fear memory, mice were placed in the conditioned fear context 24 h after fear conditioning and re-exposed to the conditioning context for 6 min without any foot shocks.

Sucrose preference test. The procedures for the sucrose preference test was similar to those described previously[32]. Briefly, mice were first single housed and habituated with two bottles of water for 1 day. Then mice were water-deprived for 24 h and were then given a choice between two bottles, one with tap water and another with 3% sucrose solution, for 24 h. Total consumption of each fluid was measured and the sucrose preference was defined as the ratio of the consumption of sucrose solution versus the consumption of both water and sucrose solution during the test.

Accelerating rotarod test. A rotarod assay of mice was done on a 6-lane belt-driven treadmill constructed for mice from Columbus Instruments as described previously[33]. Briefly, after acclimation to the instrument, mice were exercised until they were determined to be exhausted by their refusal to run despite short resting periods (<1-min rests on platform) and gentle prodding with a tongue depressor. The rotarod started at a speed of 5 rpm and progressed to 40 rpm over a 5 min period. The mean latency to fall off the rotarod for the three trials was measured. Thirteen mice from each group were pre-trained, for the first day and recorded for the next 3 consecutive days.

Prepulse inhibition (PPI). PPI test was conducted in two isolated startle chambers (MED-ASR-PRO, MED Associates, USA) as previously described[34]with a few modifications. Briefly, background noise was set at 63 dB. Each session was initiated with a block of twelve successive 125-dB habituation tones (20 ms long, intertrial interval of 15 s). These trials were used to determine the baseline. Prepulse + pulse trials consisted of a prepulse of white noise (20 ms at 0, 78, 81 or 84 dB, respectively) followed 100 ms after prepulse onset by a startling pulse (125 dB, 20 ms). These trials types were in randomized order with an average intertrial interval of 10 s (range, 5–15s). The percentage PPI induced by each prepulse intensity was calculated as [1 – (startle amplitude on prepulse trial) / (startle amplitude on pulse alone)] x 100%.

Statistical analysis. Statistical analysis was performed using GraphPad software (GraphPad Prism v6.0; GraphPad Software). Data presented as mean ± S.E.M were submitted to t-test or one-/two-way ANOVA followed by either Dunnet test, Student–Newman–Keul's test or Bonferroni's /Sidak's multiple comparisons test (as a *post hoc* test). $P < 0.05$ was considered as significant in statistics.

References

1. Matsushita, N.*, et al.* Dynamics of tyrosine hydroxylase promoter activity during midbrain dopaminergic neuron development. *J Neurochem* **82**, 295-304 (2002).

2. Cai, L.*, et al.* Ethanol-induced neurodegeneration in NRSF/REST neuronal conditional knockout mice. *Neuroscience* **181**, 196-205 (2011).

3. Sauzeau, V., Jerkic, M., Lopez-Novoa, J.M. & Bustelo, X.R. Loss of Vav2 proto-oncogene causes tachycardia and cardiovascular disease in mice. *Mol Biol Cell* **18**, 943-952 (2007).

4. Sauzeau, V.*, et al.* Vav3 proto-oncogene deficiency leads to sympathetic hyperactivity and cardiovascular dysfunction. *Nat Med* **12**, 841-845 (2006).

5. Torres, G.E.*, et al.* Functional interaction between monoamine plasma membrane transporters and the synaptic PDZ domain-containing protein PICK1. *Neuron* **30**, 121-134 (2001).

6. Kessler, M.A. & Iacovitti, L. A HUMAN MODEL SYSTEM FOR IN VITRO DEVELOPMENT OF THE DOPAMINERGIC PHENOTYPE. *Neurosci. Abst* (2000).

7. Zhou, Q., Li, J., Wang, H., Yin, Y. & Zhou, J. Identification of nigral dopaminergic neuron-enriched genes in adult rats. *Neurobiol Aging* **32**, 313-326 (2011).

8. Shu, F.*, et al.* Functional characterization of human PFTK1 as a cyclin-dependent kinase. *Proceedings of the National Academy of Sciences* **104**, 9248-9253 (2007).

9. Di Cesare, S. The Guanine Nucleotide Exchanger Vav2 Interacts with c-ErbB-2 and Induces Alveolar Morphogenesis of Mammary Epithelial Cells. (der Humboldt-Universität zu Berlin, Mathematisch-Naturwissenschaftlichen Fakultät I, 2001).

10. Granholm, A.C.*, et al.* Prenatal LPS increases inflammation in the substantia nigra of Gdnf heterozygous mice. *Brain Pathol* **21**, 330-348 (2011).

11. Shao, W.*, et al.* Suppression of neuroinflammation by astrocytic dopamine D2 receptors via alphaB-crystallin. *Nature* **494**, 90-94 (2013).

12. Tamas, P., Solti, Z. & Buday, L. Membrane-targeting is critical for the phosphorylation of Vav2 by activated EGF receptor. *Cell Signal* **13**, 475-481 (2001).

13. Sindrilaru, A.*, et al.* Wound healing defect of Vav3-/- mice due to impaired {beta}2-integrin-dependent macrophage phagocytosis of apoptotic neutrophils. *Blood* **113**, 5266-5276 (2009).

14. Shu, F.*, et al.* Functional characterization of human PFTK1 as a cyclin-dependent kinase. *Proc Natl Acad Sci U S A* **104**, 9248-9253 (2007).

15. Fetchko, M. & Stagljar, I. Application of the split-ubiquitin membrane yeast two-hybrid system to investigate membrane protein interactions. *Methods* **32**, 349-362 (2004).

16. Vargiolu, M.*, et al.* The Tyrosine Kinase Receptor RET Interacts in Vivo with Aryl Hydrocarbon Receptor-Interacting Protein to Alter Survivin Availability. *J Clin Endocr Metab* **94**, 2571-2578 (2009).

17. Egana, L.A.*, et al.* Physical and functional interaction between the dopamine transporter and the synaptic vesicle protein synaptogyrin-3. *J Neurosci* **29**, 4592-4604 (2009).

18. Hallett, P.J., Collins, T.L., Standaert, D.G. & Dunah, A.W. Biochemical fractionation of brain tissue for studies of receptor distribution and trafficking. *Curr Protoc Neurosci* **Chapter 1**, Unit 1 16 (2008).

19. Loder, M.K. & Melikian, H.E. The dopamine transporter constitutively internalizes and

recycles in a protein kinase C-regulated manner in stably transfected PC12 cell lines. *J Biol Chem* **278**, 22168-22174 (2003).

20. Gabriel, L.R.*, et al.* Dopamine transporter endocytic trafficking in striatal dopaminergic neurons: differential dependence on dynamin and the actin cytoskeleton. *J Neurosci* **33**, 17836-17846 (2013).

21. Guo, H.*, et al.* Apomorphine induces trophic factors that support fetal rat mesencephalic dopaminergic neurons in cultures. *Eur. J. Neurosci.* **16**, 1861-1870 (2002).

22. Paxinos, G. & Franklin, K.B.J. *The mouse brain in stereotaxic coordinates* (Academic Press, San Diego, 2001).

23. Zhao-Shea, R.*, et al.* Dopamine D2-receptor activation elicits akinesia, rigidity, catalepsy, and tremor in mice expressing hypersensitive {alpha}4 nicotinic receptors via a cholinergic-dependent mechanism. *FASEB J* **24**, 49-57 (2010).

24. Fernandez-Zapico, M.E.*, et al.* Ectopic expression of< i> VAV1</i> reveals an unexpected role in pancreatic cancer tumorigenesis. *Cancer cell* **7**, 39-49 (2005).

25. Ventura, A.*, et al.* Cre-lox-regulated conditional RNA interference from transgenes. *Proc Natl Acad Sci U S A* **101**, 10380-10385 (2004).

26. Auricchio, A., Hildinger, M., O'Connor, E., Gao, G.P. & Wilson, J.M. Isolation of highly infectious and pure adeno-associated virus type 2 vectors with a single-step gravity-flow column. *Hum Gene Ther* **12**, 71-76 (2001).

27. Tejomurtula, J., Lee, K.B., Tripurani, S.K., Smith, G.W. & Yao, J. Role of importin alpha8, a new member of the importin alpha family of nuclear transport proteins, in early embryonic development in cattle. *Biol Reprod* **81**, 333-342 (2009).

28. Lepekhin, E.A.*, et al.* Intermediate filaments regulate astrocyte motility. *J Neurochem* **79**, 617-625 (2001).

29. Jain, S.*, et al.* RET is dispensable for maintenance of midbrain dopaminergic neurons in adult mice. *J Neurosci* **26**, 11230-11238 (2006).

30. Sala, M.*, et al.* Behavioral and biochemical evidence of opioidergic involvement in cocaine sensitization. *J Pharmacol Exp Ther* **274**, 450-457 (1995).

31. Dai, J.X.*, et al.* Enhanced contextual fear memory in central serotonin-deficient mice. *Proc Natl Acad Sci U S A* **105**, 11981-11986 (2008).

32. Pothion, S., Bizot, J.C., Trovero, F. & Belzung, C. Strain differences in sucrose preference and in the consequences of unpredictable chronic mild stress. *Behav Brain Res* **155**, 135-146 (2004).

33. Zhu, X.*, et al.* MSC p43 required for axonal development in motor neurons. *Proc Natl Acad Sci U S A* **106**, 15944-15949 (2009).

34. Willott, J.F.*, et al.* Acoustic startle and prepulse inhibition in 40 inbred strains of mice. *Behav Neurosci* **117**, 716-727 (2003).